Check for updates

Earthquake Spectra

EARTHQUAKE ENGINEERING PRACTICE PAPER

Host-To-Target Site Response Adjustments for Site-Specific Probabilistic Seismic Hazard Analysis

Albert R. Kottke[1] | James Kaklamanos[2] | Adrian Rodriguez-Marek[3] | Robert R. Youngs[4] | Julian J. Bommer[5] | Linda Al Atik[6] | David M. Boore[7] | Suzette J. Payne[8] | Blaine M. Bockholt[9] | Glenn Russell[9]

[1]Pacific Gas & Electric Company, San Francisco, California, USA | [2]Department of Civil Engineering, Merrimack College, North Andover, Massachusetts, USA | [3]Department of Civil and Environmental Engineering, Virginia Tech, Blacksburg, Virginia, USA | [4]WSP USA, Oakland, California, USA | [5]Department of Civil and Environmental Engineering, Imperial College London, London, UK | [6]Linda Alatik Consulting, San Francisco, California, USA | [7]Consultant, Los Altos, California, USA | [8]SMJP Consulting Service, LLC, Idaho Falls, Idaho, USA | [9]Idaho National Laboratory, Idaho Falls, Idaho, USA

Correspondence: Albert R. Kottke (albert.kottke@pge.com)

Received: 25 June 2024 | **Revised:** 19 November 2025 | **Accepted:** 28 December 2025

Keywords: epistemic uncertainty | probabilistic seismic hazard analysis | site characterization | site profiles | site response analysis

ABSTRACT

An indispensable component of any site-specific probabilistic seismic hazard analysis (PSHA) is incorporating local site effects through site response analyses, rather than relying on generic amplification factors in ground-motion models (GMMs). Traditionally, the seismic hazard is calculated at a buried rock horizon and then convolved with amplification factors for the overlying layers, which requires the definition and characterization of the buried rock profile (without which neither the model for rock motions nor the site response analyses can be developed). An alternative approach is to retain the host reference rock profile in the GMM for the hazard calculations and then perform the host-to-target site response adjustment for the full profiles in a single step. This approach is illustrated by its application to a site-specific Senior Seismic Hazard Analysis Committee Level 3 PSHA for Idaho National Laboratory. The site adjustment factors are calculated using a logic-tree approach that captures the full epistemic uncertainty in these factors. This is not necessarily achieved when the logic tree only captures uncertainty in the near-surface shear-wave velocity profile. The application illustrates the use of borehole and noninvasive shear-wave velocity measurements, in conjunction with local recordings of weak earthquake motions, to constrain the logic-tree branches and their associated weights.

1 | Introduction

The ground-motion characterization (GMC) model for any site-specific probabilistic seismic hazard analysis (PSHA) must capture the complete distribution of possible ground-motion amplitudes at the site resulting from all potential earthquake scenarios envisaged in the seismic source characterization model. The distribution of possible spectral acceleration levels is referred to, in the current Senior Seismic Hazard Analysis Committee (SSHAC) guidelines (USNRC 2018), as the center, the body, and the range (CBR). The center refers to the best estimate of the expected ground-motion amplitudes; the body corresponds to the distribution of alternative models arising from different, but also technically defensible, interpretations of the available data; and the range is defined by the upper and lower bounds on the distribution. The ultimate objective is

© 2026 Earthquake Engineering Research Institute.

to develop a model that reflects the source and path characteristics of the target region and the dynamic response characteristics of the target site, calibrated to regional ground-motion and geophysical data, and to in situ measurements of the site profile. The model must also reflect the uncertainty in the characterization of the earthquake sources and the propagation paths to the site, and the dynamic response of the site, capturing the range of possible ground motions for all combinations of magnitude, distance, and oscillator frequency.

Practice in the development of GMC models has evolved considerably over the last decade, with much of the impetus for the advances being provided by site-specific PSHA studies for nuclear sites, generally conducted as high-level SSHAC projects. When the target site is not located in a region with abundant ground-motion data, it has been recognized that the center of the distribution is better captured by adjusting ground-motion models (GMMs) to the target region characteristics rather than seeking an equation that is judged to be, in some sense, inherently applicable to the target region (Bommer and Stafford 2020). To capture the body and range of the ground-motion distribution in a consistent and easily visualized manner, there has also been a general move toward the so-called backbone approach, in which the branches of the GMC logic tree are occupied by multiple versions of a single GMM, each created by applying a different adjustment to the backbone model (Bommer 2012; Atkinson et al. 2014). The two concepts of adjusting GMMs to the target region (to better capture the center of the distribution) and the backbone approach (to capture more effectively the distribution of epistemic uncertainty) are now being combined: the GMC logic tree is constructed as a series of nodes, each capturing the CBR of target-region parameters for each of adjustments for host-to-target region differences in source and path characteristics.

The dynamic response of the target site is a critical component of the GMC model and the only part of the model that can be constrained with measurements that do not depend on the occurrence of new earthquakes. At the same time, it has long been recognized that the generic amplification factors in GMMs, conditioned on V_{S30} (the time-averaged shear-wave velocity, V_S, over the uppermost 30 m at the site) and in some cases additional parameters, are very unlikely to correctly represent the amplitude and frequency characteristics for the specific site, and are associated with unacceptably high uncertainty. For these reasons, standard practice has been to develop a GMC logic tree for motions in a reference rock horizon, and then to perform site response analyses to determine the amplification factors for the overlying layers (e.g., Rodriguez-Marek et al. 2014). However, defining the interface between the rock motions and the amplification factors as a buried reference rock profile entails several challenges, including the fact that neither the GMC model for rock nor the site response model can be developed until sufficient site information has been collected to identify and characterize the reference rock profile. Moreover, it is not sufficient to assume that setting V_{S30} in the selected GMM to the value for the reference rock horizon captures the dynamic response characteristics in the rock, since the deeper profile may differ from the rock profile implicit in the GMM (Williams and Abrahamson 2021). In most site-specific PSHA studies for critical facilities, the issue has been addressed through a host-to-target adjustment made to render the GMM more applicable to the reference rock profile (e.g., Rodriguez-Marek et al. 2014). Such adjustments, however, are not straightforward since they require estimation of both V_S and damping for an inaccessible buried rock profile. To avoid the challenges associated with the intermediate step of adjusting the GMM to the reference rock horizon, several recent site-specific PSHA studies have adopted the approach of making the host-to-target adjustment in a single step, using the full profiles from the surface to the depth at which the two V_S profiles coincide (e.g., Rodriguez-Marek, Rathje, et al. 2021). In this approach, the hazard calculations are performed with a GMM adjusted to target-region source and path characteristics but without site adjustment, with subsequent application of host-to-target site adjustment factors (SAFs). This approach has the advantage that the reference rock GMC model will be applicable to all sites within a region, without the need to identify a common reference rock profile at depth (e.g., Bommer 2022).

Regarding the capture of epistemic uncertainty in site adjustment factors, it has also been realized that assigning weights to alternative V_S profiles is comparable to building a GMC logic tree with multiple GMMs, in so much that the weights are being assigned to models rather than to the outputs from the models (ground-motion amplitudes in rock or site amplification factors) that control the hazard estimates. Unintentionally narrow distributions of SAFs, for certain parameter combinations, can be avoided by adopting, in effect, a backbone approach for constructing logic trees for site response analysis (Rodriguez-Marek, Bommer, et al. 2021).

All the innovations described in the preceding paragraphs, along with several others, have recently been implemented and refined in the construction of the GMC model for an SSHAC Level 3 PSHA for the Idaho National Laboratory (INL) (Idaho National Laboratory 2022). The GMC model was developed for multiple locations at each of five facility areas on the INL site, consisting of a reference rock model combined with SAFs for each target horizon. The reference rock model was constructed using the Chiou and Youngs (2014) GMM as the backbone model, following the conclusion of Bommer and Stafford (2020) that this is the most adaptable of all current GMMs for shallow crustal seismicity. Host-region source and path characteristics were determined by Stafford et al. (2022), using the host-region V_S profile and site attenuation

19448201, 2026, 1, Downloaded from https://onlinelibrary.wiley.com/doi/10.1002/eqs4.70046 by Imperial College London, Wiley Online Library on [05/06/2026]. See the Terms and Conditions (https://onlinelibrary.wiley.com/terms-and-conditions) on Wiley Online Library for rules of use; OA articles are governed by the applicable Creative Commons License

parameter (κ_0) determined by Al Atik and Abrahamson (2021), which was retained without modification in the reference rock model, with V_{S30} set to 760 m/s. The GMC reference rock logic tree was then constructed by including a series of nodes that address host-to-target source and path differences (Boore et al. 2022; Boore 2023).

This paper presents the derivation of the final component of the GMC model, namely the SAFs to adjust the reference rock hazard to the dynamic response characteristics at the target locations. We focus on the methodological approach for the construction of the logic tree and the capture of the full epistemic uncertainty in the SAFs. Results are shown for one of the facility areas evaluated in the study. Following this introduction, we begin with a summary of available ground-motion and site characterization data compiled for the calibration of the SAFs. This is followed first by an overview of how the site response logic-tree framework is constructed, then by detailing the construction of the base-case site profiles from logic-tree branches, the approach for randomizing V_S profiles, and the selection of input motions. This is followed by a discussion of the results for the selected facility. We close with brief conclusions highlighting the key issues and challenges in applying this approach for host-to-target site adjustments.

2 | Site and Ground Motion Data

This section will describe the available site and ground-motion data used in the development of the SAFs. The methodology in this paper is intended to be broadly applicable, and the goal of this discussion is to highlight the types of data that may be available for site adjustments in PSHAs. For illustration purposes, data for one example facility area at INL will be presented: the Naval Reactors Facility (NRF). Available data include borehole lithologic logs, seismic velocity profiles, recorded ground motions, site attenuation parameter (κ_0) estimates, and modulus reduction and damping (MRD) curves.

2.1 | Site Geology

The subsurface conditions at INL are dominated by volcanic and sedimentary deposits in the Eastern Snake River Plain (ESRP). NRF is located in the central part of the INL site in the drainage basin of the Big Lost River, just to the west of the river. During periods of volcanism over the past 2.0–2.5 million years, thick sequences of basaltic lava flows were deposited throughout the region. In between volcanic events, sediments accumulated from multiple geologic processes, including alluvial and eolian sediments. Most locations on INL therefore have interbedded layers of sediments and basalts. Throughout the INL site, there are significant vertical and lateral variations in these layers that lead to considerable challenges in site characterization for ground-motion modeling (Payne et al. 2012).

For characterizing the lithology at NRF, we focused on the deepest boreholes throughout the facility area, selecting 18 boreholes from across the site (Figure 1). Nearly all boreholes in the selected dataset extend to depths greater than 130 m. Figure 2 shows the lithologic profiles associated with these boreholes, using the following generalized classification: (a) surface soil, (b) sedimentary interbed, (c) basalt, or (d) highly fractured basalt rubble. The surface soils at NRF vary in thickness from <1 to 22 m and are largely composed of gravel and sand, with silt and clay. The variability of the surface soil thickness occurs due to the irregular surfaces of basalt lava flows. Beneath the surface soil are sequences of basalt with sedimentary interbeds, which are composed of loosely consolidated sands and silts, along with clay. Boreholes indicate interbeds to depths of 500 m at NRF, and several deep, thick interbeds are continuous across the site. In Figure 2, note the continuity of the thick interbeds at depth between boreholes USGS-151 and USGS-152, which are on opposite sides of the facility area.

2.2 | Velocity Profiles

A variety of shear-wave velocity (V_S) measurements are available at NRF, including borehole-based measurements and surface-wave-based measurements, as shown in Figure 3. The borehole-based velocity data at NRF consists of a total of 21 V_S profiles available from downhole, crosshole, and suspension logging methods. Four previous seismic velocity studies provided usable V_S profiles within the footprint of NRF: Rizzo Associates (1994), (2008); STRATA Inc. (2011); and North Wind Resource Consulting, LLC, and Rizzo Associates (2015). Measurements are available to 43 m depth within the footprint of NRF, representing the surface sediments and top of basalt. As part of the INL SSHAC Level 3 PSHA, two deep boreholes were cored and logged outside of the facility area footprint (Figure 1): USGS-151 to the east of NRF; and USGS-152 to the west-northwest of NRF, in the vicinity of the NVRF seismic station (Wood Environment & Infrastructure Solutions, Inc 2021a). Downhole and suspension logging measurements were collected in both boreholes, which are critical for constraining the deeper velocity structure at NRF. In particular, the

19448201, 2026, 1, Downloaded from https://onlinelibrary.wiley.com/doi/10.1002/eqsp4.70046 by Imperial College London, Wiley Online Library on [05/06/2026]. See the Terms and Conditions (https://onlinelibrary.wiley.com/terms-and-conditions) on Wiley Online Library for rules of use; OA articles are governed by the applicable Creative Commons License

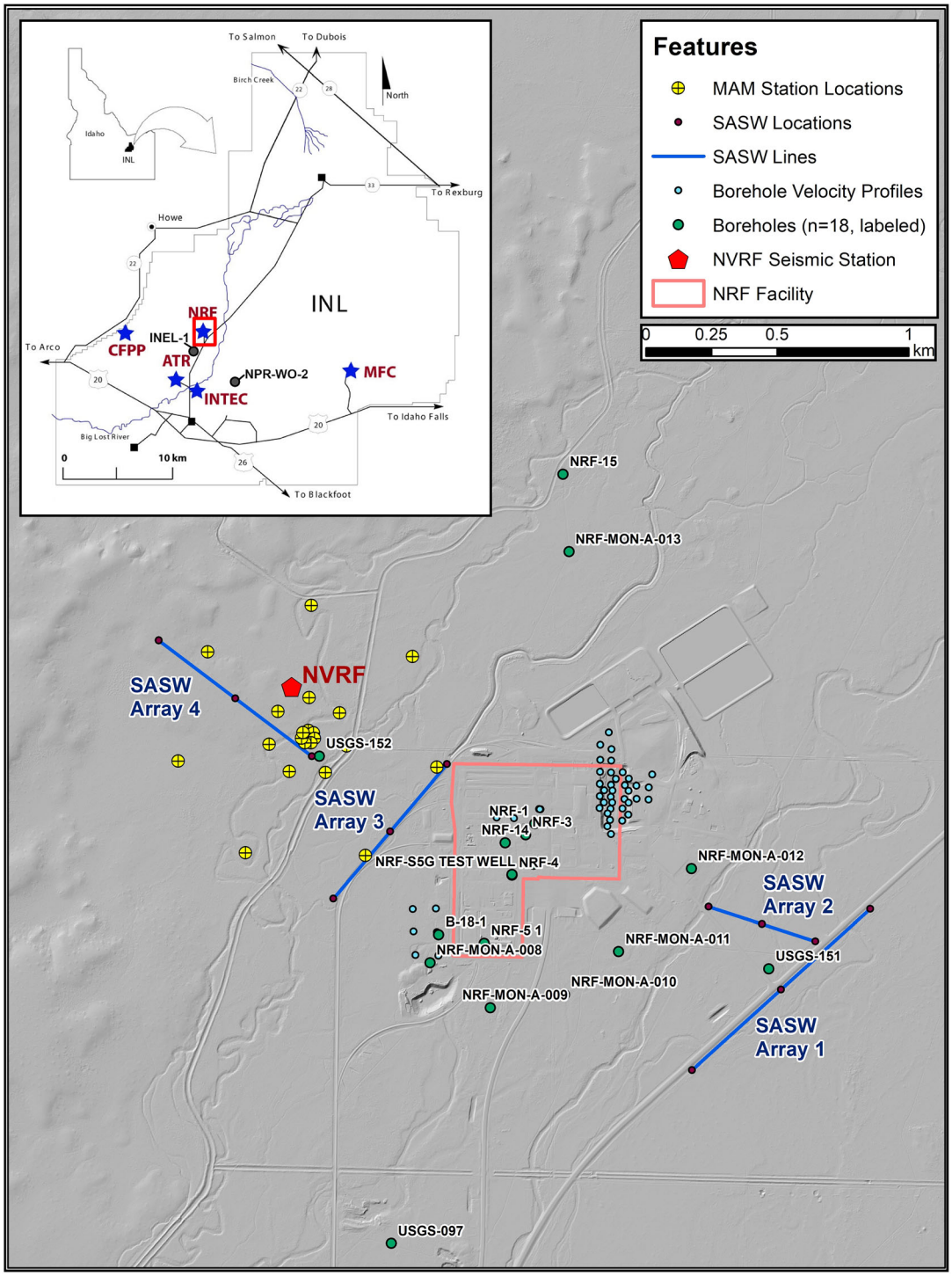

FIGURE 1 | Map of the NRF facility area and site investigation locations, including boreholes (used for lithology), borehole velocity profiles, spectral analysis of surface-wave (SASW) lines, and microtremor array measurements (MAM) arrays. The NVRF seismic station to the northwest of the facility area is also shown. The inset in the upper left corner indicates the location of NRF relative to the other facility areas and INL as a whole.

USGS-152 suspension log represents the clearest measurements of interbed velocities at INL from approximately 200 to 500 m depth.

At NRF, there are four spectral analysis of surface waves (SASW) V_S profiles (Wood Environment & Infrastructure Solutions, Inc 2021b) and six combined multichannel analysis of surface waves (MASW)/microtremor array measurements (MAM) V_S profile interpretations (Cox and Vantassel 2021). Of the four SASW lines that were measured, two were obtained to the east-southeast of NRF in the vicinity of borehole USGS-151, and two were obtained to the west-northwest

19448201, 2026, 1, Downloaded from https://onlinelibrary.wiley.com/doi/10.1002/eqsp4.70046 by Imperial College London, Wiley Online Library on [05/06/2026]. See the Terms and Conditions (https://onlinelibrary.wiley.com/terms-and-conditions) on Wiley Online Library for rules of use; OA articles are governed by the applicable Creative Commons License

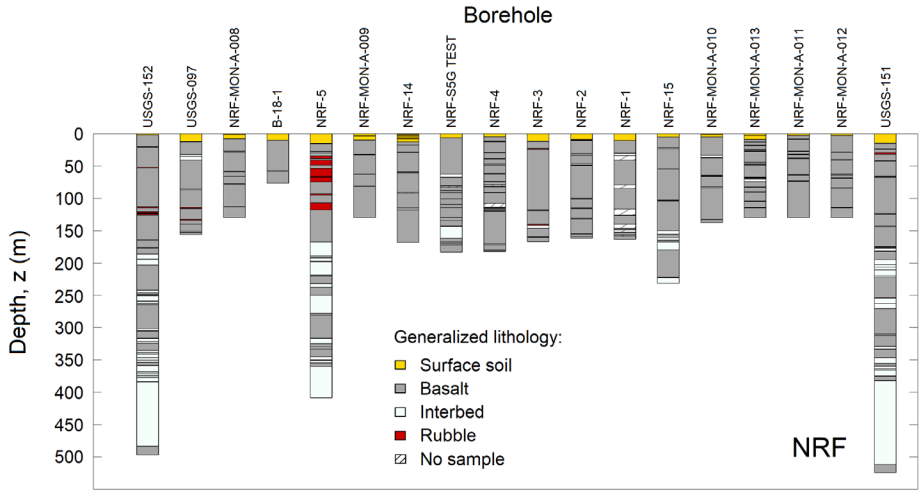

FIGURE 2 | Stratigraphic logs of the 18 boreholes in the lithology database at NRF, classified using the generalized lithology described in the text.

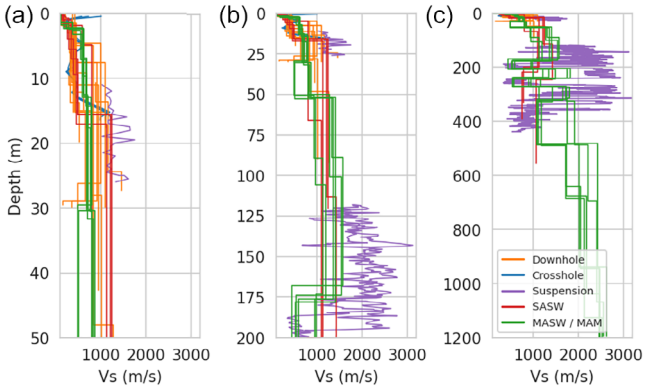

FIGURE 3 | Summary of all usable measured V_S profiles at NRF, from borehole (downhole, crosshole, and suspension) and surface-wave (SASW and MASW/MAM) methods. For the MASW/MAM profiles, only the medians from each profile type are shown. The three plots illustrate the same velocity profile data over three different depth ranges: (a) the upper 50 m, (b) the upper 200 m, and (c) the entire profile.

of NRF in the vicinity of borehole USGS-152 and the NVRF seismic station. The combined MASW/MAM measurements were collected to the northwest of the facility area, in the vicinity of borehole USGS-152, and to a maximum depth of 1,294 m. For the combined MASW and MAM dispersion curves, inverted V_S profiles were provided for dispersion curves obtained from alternative wave types (Rayleigh and Love) and alternative layering ratios (LRs) (Cox and Teague 2016). MASW/MAM inversions were also partially constrained by the lithology, which provides a higher likelihood of capturing low-velocity layers that are persistent across each site; the SASW inversions did not consider lithology. For each MASW/MAM profile interpretation, data were provided for the median profile as well as the 100 lowest misfit models. The suspension log V_S profiles tend to be greater than the SASW and MASW/MAM profiles in the basalt layers at depth. A number of factors could explain the differences between the suspension log and surface-wave profiles, including differences in material sampled, spatial averaging by the surface-wave-based methods, and/or differences in frequency sampling between the different measurement approaches.

For depths below the available site-specific velocity measurements, the deep V_S profile was constrained from two sources. First, we used velocity and lithology data from two deep boreholes measured at other INL sites (boreholes INEL-1 and NPR-WO-2) to extend the shallow V_S profiles at NRF to depths of 3.2 km. No borehole measurements across INL are available at any depths greater than 3.2 km, so the Richins et al. (1987) crustal velocity model for the ESRP was employed below 3.2 km. The Richins et al. (1987) model was originally developed for V_P and was converted to V_S, assuming a Poisson's ratio of 0.25. The use of seismological crustal velocity models in geotechnical site response analyses is not a common practice, but it allows the capture of wave propagation in the upper portion of the crust. This general approach

19448201, 2026, 1, Downloaded from https://onlinelibrary.wiley.com/doi/10.1002/eqsp4.70046 by Imperial College London, Wiley Online Library on [05/06/2026]. See the Terms and Conditions (https://onlinelibrary.wiley.com/terms-and-conditions) on Wiley Online Library for rules of use; OA articles are governed by the applicable Creative Commons License

was validated in analyses at the Garner Valley Downhole Array in California with adequate results (Rodriguez-Marek, Rathje, et al. 2021).

2.3 | Recorded Ground Motions

The ground-motion database developed for the INL SSHAC Level 3 PSHA included data from multiple local and regional networks, most significantly from the INL Seismic Monitoring Program. The database contains over 30,500 ground-motion records and spans magnitudes 3.1–6.5 and distances 9–540 km. Two significant regional earthquakes, the 2020 **M** 5.7 Magna, Utah, and the 2020 **M** 6.5 Stanley, Idaho, events, occurred during the duration of the project, strengthening the available ground-motion database. However, the vast majority of the ground-motion data consisted of small-magnitude earthquakes recorded over several years (Boore et al. 2022).

The recorded ground motion data were invaluable for calibration of the site response models, but two factors prevented the data from being utilized for empirically deriving the site adjustment factors. First, the seismic stations were often located at some distance from the target locations, and the lateral variability of the subsurface and modifications during construction meant the profiles between the target site and seismic station could be quite different. Second, in some instances, soil-structure-interaction models required the development of site-adjustment factors at a specific depth. The leveraging of ground-motion data for the inversion of crustal attenuation parameters (Silva et al. 2021) and evaluation of site response would not have been possible without the recordings from small-magnitude earthquakes, highlighting the engineering significance of weak ground-motion monitoring at critical facilities. Ground-motion data from seismic station NVRF, located to the west-northwest of the NRF facility area, were particularly important for the characterization of NRF. The station recorded 56 events with magnitudes ranging from 3.0 to 6.5.

2.4 | Site Attenuation Parameters

The host-to-target adjustments depend on the determination of several parameters of the Fourier amplitude spectra (FAS) of earthquake ground motions in the INL region. These parameters include the stress parameter $\Delta\sigma$, which controls the high-frequency energy radiated by the seismic source; crustal attenuation parameters Q_0 and η, which determine the quality factor Q according to the equation $Q = Q_0 f^{\eta}$, where f is frequency; and site attenuation parameter (κ_0), which determines the attenuation of high-frequency energy in the FAS of ground motion for each recording station, as given by the expression $\exp(-\pi\kappa_0 f)$. These parameters were determined by inversions of ground-motion recordings obtained in the INL region (Silva et al. 2021). The parameters Q and $\Delta\sigma$ are part of the reference rock model and are described in detail by Boore et al. (2022). On the other hand, κ_0 is related to site response and thus is part of the site response calculation. There are different ways in which κ_0 can be interpreted, but we assume that κ_0 is primarily associated with material damping within layers, as well as scattering at layer boundaries. Therefore, all soil profiles were assigned small-strain damping ratios such that the total effect of material damping and scattering in the one-dimensional (1D) soil column replicated the value of the target κ_0. This approach, described further in the Target κ_0 section, ensured consistency between the damping model in site response analyses and the high-frequency attenuation seen in the observed ground motions.

Combining analytical site amplification factors with κ_0 to define site-specific amplification functions has inherent limitations. This method depends on analytical modeling to accurately represent local site effects and assumes that κ_0 reflects only site-related influences. While direct use of ground motion data (e.g., Hassani et al. 2025) could yield site corrections with lower uncertainty, it is impractical for these locations due to varying foundation conditions. Moreover, if any component of κ_0 is actually a magnitude-dependent source effect, both approaches are compromised by this assumption. Despite these limitations, it offers the ability to constrain the high-frequency attenuation based on empirical data.

The inversion analyses determined that the values of the parameter η are correlated with the values of κ_0 (Silva et al. 2021). The reference rock GMM logic tree included five branches to capture the uncertainty in η. To ensure that this correlation is captured correctly, five central values of κ_0 (0.0412, 0.0462, 0.0525, 0.0572, and 0.0606 s), one for each η value in the reference rock GMM logic tree (0.50, 0.53, 0.56, 0.58, and 0.60, respectively), were determined for each site. The central values of κ_0 were obtained from an inversion of regional ground motion recordings. These inversions considered different η values, which resulted in different central κ_0 values.

19448201, 2026, 1, Downloaded from https://onlinelibrary.wiley.com/doi/10.1002/eqs4.70046 by Imperial College London, Wiley Online Library on [05/06/2026]. See the Terms and Conditions (https://onlinelibrary.wiley.com/terms-and-conditions) on Wiley Online Library for rules of use; OA articles are governed by the applicable Creative Commons License

2.5 | MRD Data and Models

MRD curves are needed to characterize the nonlinear behavior of soils within the equivalent-linear site response framework, which we employed in the site response calculations. MRD curves are generally developed from the results of dynamic laboratory testing; however, the careful sampling and testing needed to develop MRD curves are expensive and require a particular expertise. For this reason, many projects opt for the use of generic models for MRD curves published in the literature (e.g., Darendeli 2001 [D01]; Menq 2003; Wang and Stokoe 2022 [WS22]). These generic models are generally developed from large numbers of dynamic tests on intact or reconstituted samples, and are keyed to index properties of soils. An advantage of a generic model, such as D01, is that it is based on a large number of tests on soils that span a wide range of index properties and a range of stress state conditions.

Several testing programs for obtaining MRD curves were conducted for surface soil and interbeds at NRF, predominantly using resonant column and torsional shear testing (North Wind Resource Consulting, LLC, and Rizzo Associates 2015; Wood & University of Texas at Austin 2022). INL-specific models were derived by fitting the parameters of the WS22 MRD functional form to these data (Figure 4).

In addition to surface soil and interbeds, the potential nonlinear response of the basalt and rubble in the upper portion of the profile must also be considered. North Wind Resource Consulting, LLC, and Rizzo Associates (2015) presented measurements from multiple basalt samples at NRF. These basalt MRD models were developed by fitting the Darendeli (2001) functional form, which is versatile in nature, to the dynamic testing data on basalt samples at NRF. Given the absence of MRD curves for highly fractured basalt, these MRD curves were also employed in layers characterized as rubble.

3 | Site Response Logic-Tree Approach

The approach used to capture the epistemic uncertainty (i.e., center, body, and range) of the site adjustment factors (SAFs) is the site response logic-tree approach. SAFs are defined as the ratio of predicted spectral acceleration at the surface of the target profile to that of a V_S profile compatible with the reference rock GMM (i.e., the "host profile"). Key to this approach is that the epistemic uncertainty in all the elements that are needed to compute SAFs is represented in a site response logic tree, but SAFs that result from the logic tree are resampled into a discrete number of branches (Rodriguez-Marek, Bommer, et al. 2021). The resampling process implies that the computational cost of additional branches in the site response logic-tree is not transferred to an additional cost in the hazard computation. A second benefit is that the tools

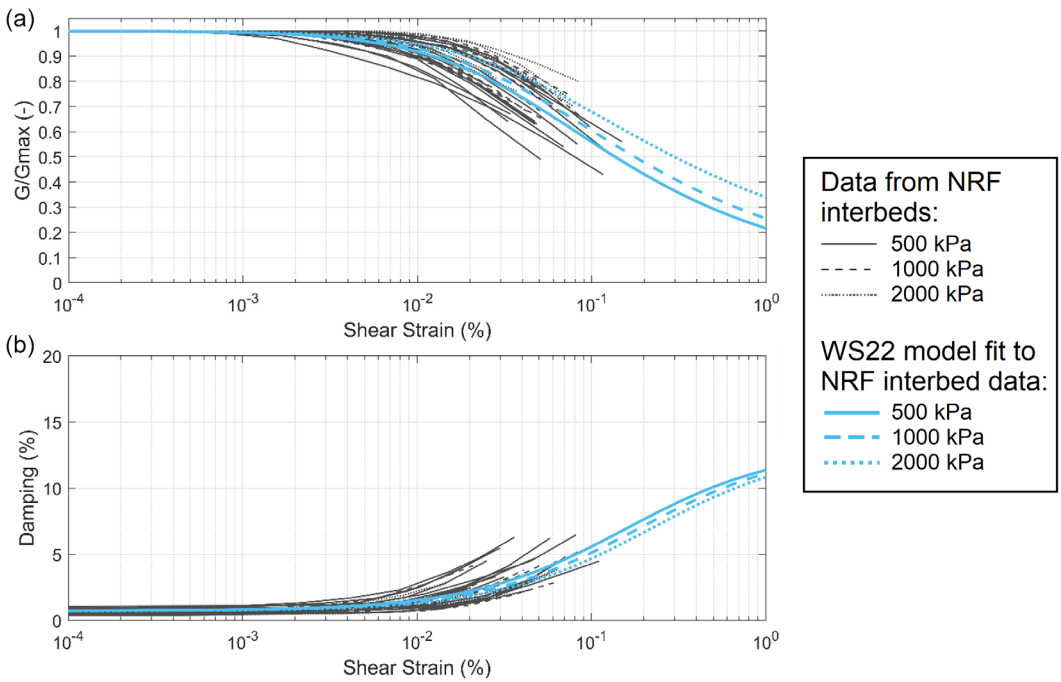

FIGURE 4 | MRD data from interbed samples from NRF compared with the WS22 model fitted to these data. The WS22 model allows for confining stress as an input, and is plotted for selected confining stresses (500, 1000, and 2000 kPa). The linetype for each of the data curves matches that of the closest confining stress used for the models.

19448201, 2026, 1, Downloaded from https://onlinelibrary.wiley.com/doi/10.1002/eqs4.70046 by Imperial College London, Wiley Online Library on [05/06/2026]. See the Terms and Conditions (https://onlinelibrary.wiley.com/terms-and-conditions) on Wiley Online Library for rules of use; OA articles are governed by the applicable Creative Commons License

to explore the sensitivities of logic trees in PSHA (i.e., tornado plots and variance contribution plots) can be used to explore which components of the logic tree have the highest impact on the uncertainty in the SAFs. In the development of a logic tree, it is important to consider potential correlations between branches to prevent an unintended wide distribution of alternatives.

Site adjustment factors are computed by performing site response analyses for both the host and target profiles. Both the host and target profiles include details of the V_S and damping profiles in what is termed the "one-step" approach, as recommended by Williams and Abrahamson (2021). The adopted approach is summarized as:

- Velocity profiles are defined for the host regions (crustal and subduction).
- Target velocity profiles are constructed using a logic tree approach to capture all relevant sources of epistemic uncertainty. Both the host and target profiles are constructed to the depth of the source V_S (3,550 m/s) or to a depth large enough that all possible influences on the SAF at the longest oscillator period under consideration (10 s) are included.
- The site response of the host profiles is assumed to be linear. The impact of nonlinearity on ground motions at the target sites is fully captured in the site response analyses for the target profiles.
- Site adjustment factors are computed as the ratio of ground motions between the host and target profiles for each branch of the logic tree. The SAFs capture both intensity and magnitude dependence. Intensity dependence is quantified by having the SAFs be dependent on the intensity of the ground motions at the reference rock. The computation of SAFs for each branch of the logic tree involves randomization of the target V_S profile to incorporate the aleatory variability in SAFs.
- Where applicable, the SAFs are modified to account for non-1D effects.
- Following Miller and Rice (1983), the SAFs are resampled into seven discrete branches for each target period. The resampling process includes considerations of model error. The resampled SAFs are intended to preserve the mean and variance of the full logic tree distribution (Rodriguez-Marek, Bommer, et al. 2021).

The site-response logic tree for the NRF facility is shown in Figure 5. The following subsections discuss elements of the logic tree, including the host V_S profiles, the target value of κ_0, and the choice of MRD curves. Details on the construction of base-case V_S profiles are given in a separate section, followed by a section explaining the approach adopted to include randomization around the base-case V_S profiles. Each branch of the logic tree is assigned a weight determined by the GMC Technical Integration team (GMC TI team); the following sections also include a discussion on the approach adopted by the GMC TI team for the assignment of weights.

3.1 | Host Profile and κ_0

The host V_S profile is obtained using the approach developed by Al Atik and Abrahamson (2021), where a 1D V_S profile is constructed such that its predicted site response with respect to a reference profile is consistent with the implicit V_{S30}

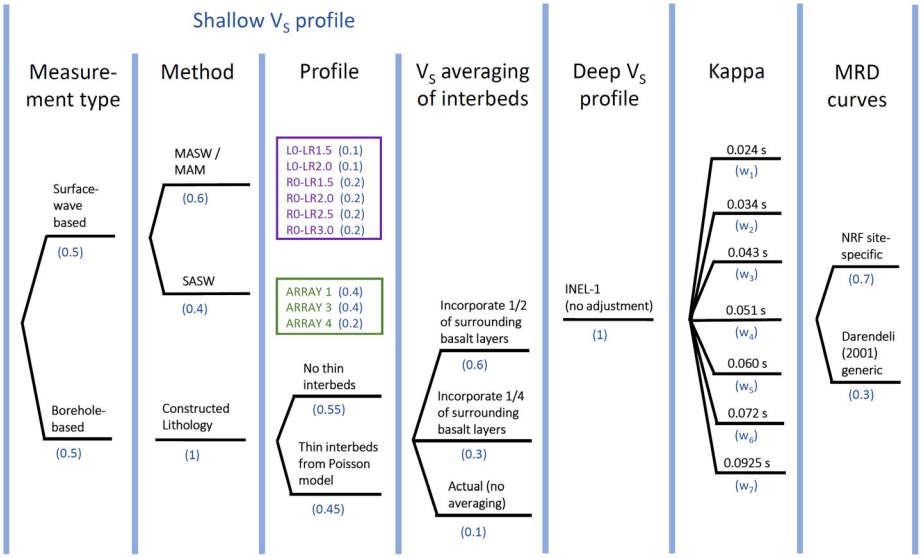

FIGURE 5 | Full logic tree for the NRF site profiles, with numbers in parentheses denoting the weights on each branch. The basis for the weights for the site kappa node is further described in the Target κ_0 section.

19448201, 2026, 1, Downloaded from https://onlinelibrary.wiley.com/doi/10.1002/eqs4.70046 by Imperial College London, Wiley Online Library on [05/06/2026]. See the Terms and Conditions (https://onlinelibrary.wiley.com/terms-and-conditions) on Wiley Online Library for rules of use; OA articles are governed by the applicable Creative Commons License

scaling of the host GMM. As indicated before, the host GMM for crustal earthquake sources is the Chiou and Youngs (2014) model for a V_{S30} value of 760 m/s. The INL source characterization model also included sources other than shallow crustal earthquakes (volcanic sources and subduction sources); however, this paper focuses exclusively on the SAFs for crustal sources. Site response is estimated using the quarter-wavelength method of Boore (2003). The Al Atik and Abrahamson (2021) approach was also used to determine the host κ_0 value corresponding to the host GMM model; this value is 0.039 s. The option to include epistemic uncertainty in the host profile was extensively discussed. However, the GMC TI team decided against including uncertainty in the host profile (in crustal amplification and in κ_0). The primary reason is that the objective is to have sufficient uncertainty in the entire adjustment, and since the uncertainty in the host model is relatively small (because the crustal amplification of the host profile is a network average), it was sufficient to include uncertainty in the target profile only.

3.2 | Target κ_0

The approach used to constrain κ_0 values was discussed in the *Site Attenuation Parameters* section. In addition to the central values of κ_0, the epistemic uncertainty of κ_0 is needed. To facilitate the quantification of this uncertainty, additional estimates of κ_0 using alternative methodologies were performed at the MFCF seismic station near the MFC (Materials and Fuels Complex) facility area (see inset map in Figure 1); refer to Idaho National Laboratory (2022) or Silva et al. (2021) for details. The epistemic uncertainty in κ_0 was then quantified using a combination of the values of the inversion at each facility area and the method-to-method variability in the uncertainty in κ_0 computed for the MFCF station.

The epistemic uncertainty in κ_0 was computed by combining the between-method uncertainty and the within-method uncertainty:

$$\sigma_{\ln\kappa} = \sqrt{(\sigma_{\ln\kappa\,-\,\text{within method}})^2 + (\sigma_{\ln\kappa\,-\,\text{between method}})^2} \tag{1}$$

The application of this equation with the measured values at the MFCF station resulted in values of $\sigma_{\ln\kappa}$ ranging from 0.20 to 0.30. Judging that an intermediate value is appropriate, the GMC TI Team set the epistemic uncertainty of κ_0 for the NRF site to 0.25. Note that this value is smaller than the 0.4 value recommended in EPRI (2013), the reduction being justified by the extensive number of ground-motion records at the INL sites. The epistemic uncertainty in κ_0 is captured using a seven-point distribution (Miller and Rice 1983), with weights applied to these seven κ_0 values such that the distribution captures the target median and standard deviations. As indicated before, the central value of κ_0 is linked to the η branch of the reference rock logic tree. As a practical choice, the site response analyses were only conducted using seven values of κ_0. Therefore, weights for each branch of the κ_0 logic tree were modified to achieve the desired central κ_0 value. The correlation with the path parameter η is modeled by linking the kappa node in the site response logic-tree with the η node in the reference rock motion logic-tree. Further details are provided in Idaho National Laboratory (2022) and Silva et al. (2021).

A final component of the κ_0 logic tree node relates to the correlation between shear-wave velocity profiles and κ_0. Silva et al. (2021) performed broadband inversions that simultaneously fit source, path, and site terms to FAS data. These inversions include site effects via computed site factors using estimated V_S profiles. If the records at a station imply site terms with large amplitudes at high frequencies, these high amplitudes can be explained either by strong high-frequency amplification due to site effects, or by low site κ_0. Therefore, if a profile used in the inversion would predict higher-than-average amplification, it would be associated with higher-than-average κ_0. Conversely, if a profile used in the inversion would predict lower-than-average amplification, it would be associated with lower-than-average κ_0.

These considerations point to a positive correlation between the predicted amplification at high frequencies and the κ_0 assigned to a profile. The correlation is expected to be strong given that the measured high-frequency portion of the spectrum can be equally explained by low/high site amplification and low/high κ_0 values. This correlation is imposed on the logic tree by first running preliminary site response analyses using the κ_0 logic tree values as described above. For each branch of the logic tree that affects the values of V_S (i.e., the first four nodes for the NRF site; Figure 5), an epsilon value ε_{SAF} is computed using:

$$(\varepsilon_{SAF})_i = \frac{\ln \text{SAF}_i - \ln \text{SAF}_{\text{median}}}{\sigma_{ep}} \tag{2}$$

19448201, 2026, 1, Downloaded from https://onlinelibrary.wiley.com/doi/10.1002/eqs4.70046 by Imperial College London, Wiley Online Library on [05/06/2026]. See the Terms and Conditions (https://onlinelibrary.wiley.com/terms-and-conditions) on Wiley Online Library for rules of use; OA articles are governed by the applicable Creative Commons License

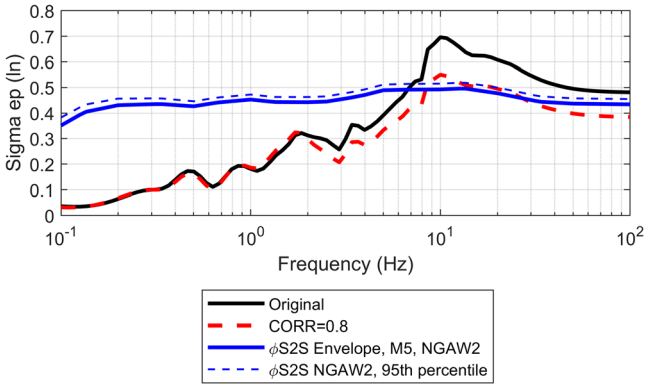

FIGURE 6 | Epistemic uncertainty computed from a preliminary version of the NRF site response logic tree. The black solid line is the uncertainty of the original logic tree, the dashed red line is the epistemic uncertainty after imposing a correlation of 0.8 between SAF and κ_0. The blue lines correspond to the envelope of the network average site-to-site variability of four NGA West 2 GMMs (Abrahamson et al. 2014; Boore et al. 2014; Campbell and Bozorgnia 2014; and Chiou and Youngs 2014).

where SAF_i is the conditional weighted mean SAF for branch i, and SAF_{median} and σ_{ep} are the median and the standard deviations of the SAFs computed from the site response logic-tree, respectively. Once ε_{SAF} is computed, the median kappa value for each branch of the logic tree (k_i) is modified using:

$$\ln \kappa_i = \ln \kappa_0 + \mathrm{CORR} \cdot (\varepsilon_{SAF})_i \cdot \sigma_{\ln\kappa} \tag{3}$$

where the median kappa value (κ_0) and the standard deviation of kappa ($\sigma_{\ln\kappa}$) are determined as described previously in this section, and CORR is the correlation between ε_{SAF} and κ_0. This methodology changes the central value of κ_0 for each branch of the logic tree, resulting in an overall decrease of the resulting epistemic uncertainty in the SAFs without a change in the median SAF values. An example result for the NRF site is given in Figure 6 for CORR = 0.8; the resulting epistemic uncertainty in the SAF is reduced for high frequencies and is comparable with the site-to-site variability in the NGA West2 models (Bozorgnia et al. 2014) at high frequencies. While there are no data to constrain the actual value of the CORR parameter, the GMC TI team selected the value of 0.8, given that it reduced the epistemic uncertainty in SAF to the site-to-site variability (ϕ_{S2S}) in the NGA West2 models. The GMC TI Team considered the NGA-West2 epistemic uncertainty to be a reasonable upper bound for SAFs, given the limited site characterization of recording stations in the NGA West2 database compared to the level of characterization at the INL sites.

3.3 | MRD Curves

The available MRD models were discussed in the previous section on Site and Ground Motion Data. As described therein, there are two sets of models available for surface soils and interbeds: an INL-specific (the modified WS22 model) and the Darendeli (2001) model. The choice of the MRD model is given its own node in the site response logic tree, with branches for the INL-specific and D01 models having weights of 0.7 and 0.3, respectively. For the NRF site, the INL-specific model is given higher weight because it is built primarily from samples from the NRF site (Figure 4).

A single set of MRD curves was used for the basalt and the rubble layers; due to the minimal level of nonlinear behavior in these layers, the choice of the basalt and rubble MRD models has a negligible impact on the site response results.

4 | Construction of Base-Case Profiles

The V_S profiles used to develop the SAFs were created through a consideration of alternative decisions based on target-specific logic trees (e.g., Figure 5) and stochastic randomization included to account for aleatory variability. For the analyses performed in this study, the V_S profile extends to a depth of 6.5–8 km and is terminated at the depth where V_S equals the source velocity of 3,550 m/s. The profile is comprised of four sections:

1. Near-surface soil profile,
2. Shallow-velocity profile based on lithology and surface-wave-based measurements,
3. Deep-velocity profile based on two approximately 3-km-deep borings, and
4. Crustal velocity profile that extends to the source depth.

19448201, 2026, 1, Downloaded from https://onlinelibrary.wiley.com/doi/10.1002/eqs4.70046 by Imperial College London, Wiley Online Library on [05/06/2026]. See the Terms and Conditions (https://onlinelibrary.wiley.com/terms-and-conditions) on Wiley Online Library for rules of use; OA articles are governed by the applicable Creative Commons License

Each of these profile segments is spliced together to create a final velocity profile. Alternatives can be sampled through the modification of each of the segments. Each velocity within the base-case profile is considered to be an estimate of the median.

4.1 | Near-Surface Soil Profile

The near-surface soil is only present under some of the buildings considered, but it is some of the most poorly characterized material. Additionally, security restrictions prevented the characterization of the velocity profile in the immediate vicinity of the buildings. Therefore, data from multiple sources are used to create an INL-wide depth-dependent velocity model for near-surface soil. The depth of the base of near-surface soil is assessed on a site-specific basis, and if uncertain, can be sampled from a distribution. At NRF, the thickness of the near-surface soil ranges from 0 to 12.2 m at the hazard targets of interest.

4.2 | Shallow Velocity Profile

The GMC TI team decided to construct shallow V_S profiles separately from information gathered from surface-wave measurements and borehole measurements. These two approaches represent two distinct ways of determining V_S profiles. Shear-wave velocity profiles obtained from measured surface-wave dispersion curves imply an averaging over a large volume of soil; this volume is on the scale of the size of the array and varies depending on the depth (i.e., the wavelength of measurements). This is considered an advantage of these methods because site response at a site is also affected by velocity profiles away from the location where the site response is being measured (Hallal and Cox 2021, 2023). That said, the inversion process for surface-wave measurements is nonunique, and velocity reversals (which are known to exist at INL sites) are difficult to capture. Shear-wave velocity profiles obtained from borehole measurements capture better the details in the vertical variation of V_S profiles. On the other hand, borehole-based profiles are point measurements of the V_S and the lithology, and thus ignore the lateral variability over the site. The weights for both approaches (surface vs. borehole-based) are assigned to be equal. The following subsections describe separately the construction of lithology-based profiles and surface wave-based profiles, which were constructed separately for profiles measured with MASW/MAM and the SASW approaches.

4.2.1 | Lithology-Based Profiles

The lithology-based profiles are constructed from two components: a best-estimate lithology profile and lithology-specific models for velocity and density. The lithology profile was developed through interpretation of multiple boreholes over the area surrounding a target location (e.g., Figure 2). This information was used to identify persistent thick interbeds that are common in nearly all borings, and stochastic thin interbeds that vary from one boring to the next. For persistent thick interbeds, the thickness of the interbeds is considered to be spatially variable, and the thickness is randomly varied based on the evaluation of the repeated sampling of interbeds. For profiles with stochastic thin interbeds, the borings were used to calibrate two probabilistic distributions: a nonhomogeneous Poisson model for the occurrence rate of interbeds, and a shifted Beta distribution for the thickness of interbeds. These models were used for the random generation of interbeds.

In the site response logic tree, the GMC TI team considered branches with and without stochastic thin interbeds (Figure 5), with a weak preference for the model without thin interbeds (weights of 0.55 and 0.45, respectively). The primary reason for this choice is that the modeling of thin interbeds in 1D site response unduly exaggerates their impact, because the lateral continuity of layers is assumed in a 1D model. However, the thin interbeds option is retained because these features are clearly present in nearly all the boreholes that were logged at the INL facility and are also seen in V_S profiles constructed with suspension logging.

For a given lithology, the velocity and density were assigned based on models developed for the INL site. Since little uncertainty is associated with density, we adopted a single model for assigning density, using site-specific data from INL (Payne et al. 2012), as well as a generic model from Boore (2016). Lithology-specific and depth-dependent velocity models were developed through interpretation of borehole-based velocity measurements.

There are two commonly used functional forms to characterize the depth-dependent increase in the velocity of a homogenous material. The first model is the power-law model:

$$V_S = \theta_1 z^{\theta_2} \tag{4}$$

19448201, 2026, 1, Downloaded from https://onlinelibrary.wiley.com/doi/10.1002/eqs4.70046 by Imperial College London, Wiley Online Library on [05/06/2026]. See the Terms and Conditions (https://onlinelibrary.wiley.com/terms-and-conditions) on Wiley Online Library for rules of use; OA articles are governed by the applicable Creative Commons License

where depth (z) is substituted for stress from the model first proposed by Hardin and Richart (1963), and parameters θ_1 and θ_2 are fitted to the data. This model is commonly used for soils for which the velocity increases with depth. The second model, referred to as the exponential model, is based on rock mechanics concepts (Mavko and Vanorio 2010), and is defined as:

$$V_S = \theta_1 \left[1 - \theta_2 \exp\left(-\frac{z}{\theta_3} \right) \right] \tag{5}$$

where θ_1, θ_2, and θ_3 are three fitting parameters. This model approaches a maximum value of θ_1 at depth.

Using the borehole-based velocity data, each data point was assigned a lithology as surficial soil, interbed, fractured basalt (rubble), intact basalt, or rhyolite, based on drilling logs, as shown in Figure 7a. However, there are overlaps in the velocity distributions for different lithologies, and some of the units (such as rubble) have minimal measurements. These observations complicate the development of lithology-based velocity models. To overcome these challenges, an approach is used to develop new lithology-based V_S correlations where the lithology is selected as part of the fit of the model. This process is used to simultaneously develop models for the interbed, rubble, and basalt; the near-surface soil is treated separately with a specified power-law model, depending on the site-specific thickness of surface soil at the hazard targets.

The simultaneous regression is performed using a mixture model with three different velocity models in log-velocity and log-depth space using *pymc3* (Salvatier et al. 2016) with Bayesian Markov chain Monte Carlo (MCMC) methods. In the MCMC method, prior information is included in the modeling process by defining the distribution of the parameters. Both the power-law (Equation (4)) and exponential (Equation (5)) models were tested for each material type. Ultimately, a power-law model was used for the rubble, and exponential models were used for both interbeds and basalt. At a depth of 20 m, the interbed velocity is limited to be less than the rubble velocity, and the rubble velocity is limited to be less than the basalt velocity. For each of the velocity models, the prior distributions of the parameters were modeled as a lognormal distribution with a median defined from the unit-specific regressions and a standard deviation of 0.05. The results of the regressions are shown in Figure 7b. The logarithmic standard deviation of the fit is assumed equal for all three material types; the computed value is 0.197.

4.2.2 | SASW Profiles

At the NRF facility area, there were four SASW test locations (Figure 1), and one SASW profile was provided for each location. The GMC TI Team eliminated Array 2 from the logic tree because the profile truncates at a relatively shallow depth compared to the other profiles, and it is largely consistent with Array 1 over the range it samples. The site response logic-tree included one branch for each of the three remaining test locations (Arrays 1, 3, and 4), with weights assigned based on proximity to the target site. In some instances, the resulting velocity profiles included low-velocity zones, which were inconsistent with the boring information near the target locations. The low-velocity zones were adjusted by using

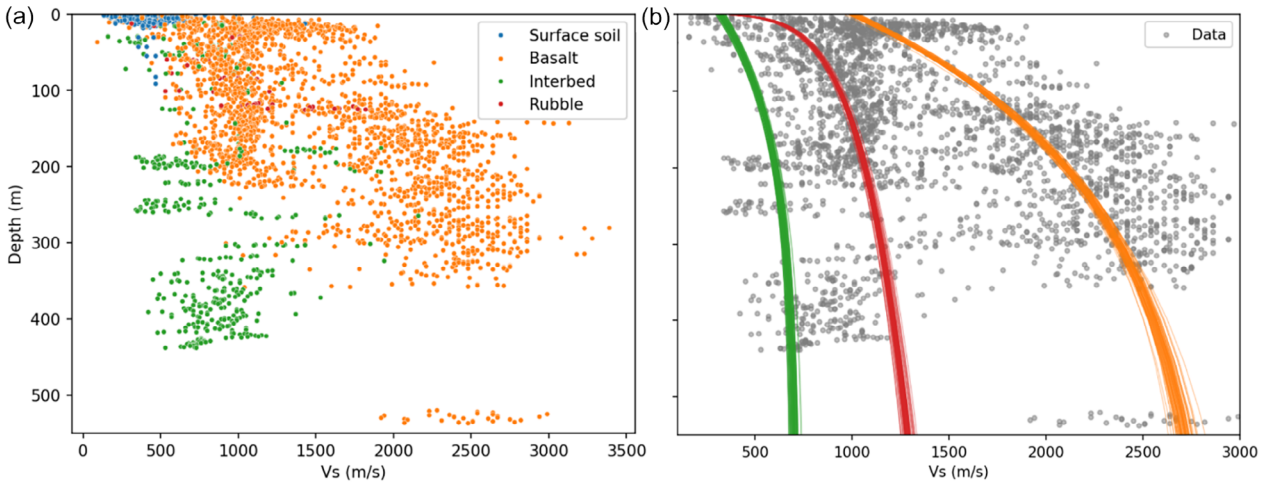

FIGURE 7 | (a) Comparison of the borehole velocity measurements between lithologies at all INL facilities, and (b) fits of the three models: Interbed (orange), Rubble (green), and Basalt (red) to the borehole velocity measurements. The alternative models in part (b) illustrate the overall stability of the model, but only the mean value is used in the application.

19448201, 2026, 1, Downloaded from https://onlinelibrary.wiley.com/doi/10.1002/eqs4.70046 by Imperial College London, Wiley Online Library on [05/06/2026]. See the Terms and Conditions (https://onlinelibrary.wiley.com/terms-and-conditions) on Wiley Online Library for rules of use; OA articles are governed by the applicable Creative Commons License

the median rubble velocity model as a minimum velocity to adjust the SASW profile to match the ground conditions. This was considered an acceptable adjustment given that it resulted in minor modifications to the profile, while maintaining consistency with the target site conditions.

4.2.3 | MASW/MAM Profiles

MASW/MAM measurements were performed in one array northwest of the facility area (Figure 1). The array was analyzed using both fundamental-mode Rayleigh wave (R0) and fundamental-mode Love wave (L0) dispersion data, using an inversion approach that allowed for alternative layering ratios, which modulate the number of possible layers that exist in the subsurface. The site response logic-tree included one branch for each measurement approach (Rayleigh vs. Love waves) and each alternative layering ratio. Weights were assigned based on the confidence of the GMC TI Team in the alternative inversion approaches. Greater weight was applied to the Rayleigh-wave data because the knowledge base and experience with Rayleigh-wave data is significantly greater than that of Love-wave data, and the Love-wave target fundamental dispersion curves exhibited patterns markedly different than all other surface-wave profiles. For each inversion, the data processing of the MASW/MAM provided 100 alternative velocity profiles that were intended to sample across the inversion uncertainty (Cox and Vantassel 2021). The first 60 of these profiles were selected for use in defining the base-case profile, and material types were assigned based on the lithology-based velocity model. The GMC TI team assigned a higher weight to the MASW/MAM measurements (0.6) than the SASW measurements (0.4) because the coupling of MAM with MASW allowed for an improved definition of profiles to a larger depth, and the inversion of the MASW/MAM dispersion curves was partially guided by the lithology at each site.

4.3 | Deep Velocity Profile

Beneath the shallow velocity profile, the upper portion of the deep velocity profile was constructed using data from the two deepest boreholes measured at the INL site: INEL-1 and NPR-WO-2. Two branches for the deep velocity profile in the site response logic tree represent the alternatives of (1) the INEL-1 deep profile, or (2) a profile constructed by splicing the NPR-WO-2 profile with the INEL-1 profile. The weights are assigned to each profile as a function of the expected similarity between the site's geology and the geology for each of these two deep boreholes, and the similarity between the estimated thicknesses of basalt layers between each site and each borehole (Whitehead 1992; McLing et al. 2014). The GMC TI team ultimately opted to include one deep velocity profile alternative at NRF, namely the INEL-1 velocity profile, with a weight of unity. The basis for this decision was the relatively close proximity of the site to the INEL-1 borehole and the results of sensitivity analyses that showed that this branch of the logic tree did not reduce the epistemic uncertainty in the SAFs.

4.4 | Crustal Velocity Profile

Beneath the borehole-based deep V_S profile, the bottom portion of the V_S profile is constructed from crustal velocity models. The model by Richins et al. (1987) was selected because it has precedence for its application at the INL site (Idaho National Laboratory 2016). Initial sensitivity studies by the GMC TI team showed that this deep portion of the profile does not affect the SAFs significantly at the surface; thus, no epistemic uncertainty was added to the crustal portion of the deep V_S profile.

4.5 | Example Construction

The near-surface soil profile based on soil depth information for a specific building is joined with the shallow-velocity profile by replacing layers in the shallow-velocity profile with the velocity model for surficial soil. The deep-velocity profile is appended to the bottom of the shallow-velocity profile; potential resonances at this boundary are reduced by a gradual transition between the shallow and the deep profiles. The gradual transition occurs over five transitional layers between the two profiles, and the velocities of these transitional layers are equally spaced in log-velocity. The final component is the crustal velocity profile that extends to the half-space of the site response model. The crustal velocity profile is appended to the base of the deep velocity profile. The crustal velocity profile is not considered to have strong depth-dependent characteristics; thus, a more robust transition approach is used in which the crustal velocity profile is shifted in depth. This shifting is performed such that the next layer in the velocity profile is the next-higher velocity layer in the crustal model. If the maximum velocity in the shallow-velocity profile exceeds the crustal model, then no additional layers are appended.

19448201, 2026, 1, Downloaded from https://onlinelibrary.wiley.com/doi/10.1002/eqs4.70046 by Imperial College London, Wiley Online Library on [05/06/2026]. See the Terms and Conditions (https://onlinelibrary.wiley.com/terms-and-conditions) on Wiley Online Library for rules of use; OA articles are governed by the applicable Creative Commons License

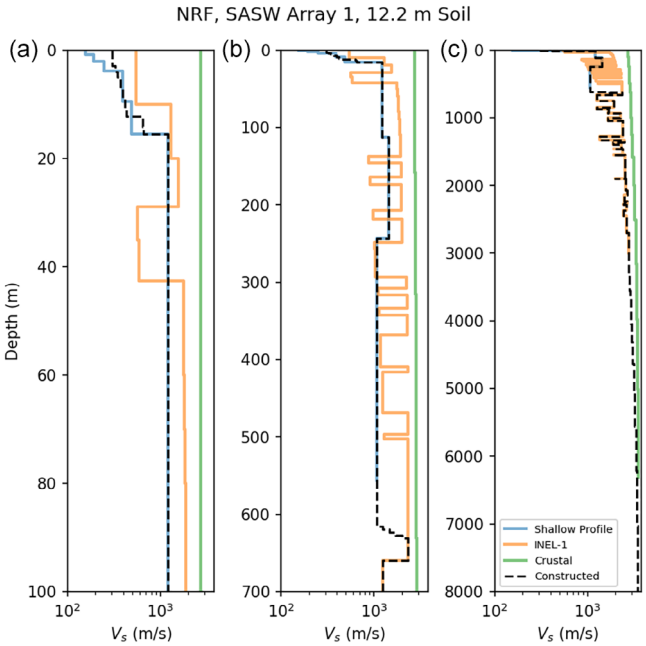

FIGURE 8 | Example construction of the NRF profile using SASW Array 1 with 12.2 m of soil, illustrated over three depth ranges: (a) upper 100 m, (b) upper 700 m, and (c) the entire profile.

To better understand the construction process, two profiles are used for illustration. The construction process for the NRF profile using SASW Array 1 with 12.2 m of surface soil is shown in Figure 8. At depths less than 15.5 m, the layers are classified as soil in the original SASW profile, and are replaced as follows: at depths less than 12.2 m (the target soil thickness), the layers are replaced with an INL-specific surficial soil velocity model; and between 12.2 and 15.5 m, the velocities are replaced with velocities computed by the depth-dependent rubble model. Between depths of 15.5 and 600 m, the profile corresponds to the original SASW Array 1 profile. At the base of the shallow profile (around 600 m), the profile transitions to the INEL-1 profile, which then transitions to the crustal model at around 3 km depth. The construction of the NRF profile using lithology with stochastic thin interbeds, assuming 0 m of surface soil, is shown in Figure 9. In the upper 120 m, the generation of the rubble zones can be seen in the profile; for each zone, lithology (i.e., basalt or rubble) was randomly assigned based on the proportions observed in the borehole velocity data. From depths of 180–500 m, three thick interbeds constrained from borehole logs are visible in the profile; furthermore, between 250 and 380 m, the thin interbeds generated during the construction of the profile can be observed. At a depth of 580 m, the profile transitions to the INEL-1 model before transitioning to the crustal model at around 6 km depth.

5 | Treatment of Aleatory Variability and Site Response

In this section, we describe some of the novel aspects of our treatment of aleatory variability and site response in the adopted site adjustment model. The use of the full-resonance amplification approach introduces sharp peaks in response at resonance frequencies defined by the 1D layered crustal velocity profile. The common practice in assessing ground motions for nuclear facilities is to account for the potential for lateral variations in layering and shear-wave velocity over the footprint of a nuclear facility by randomizing the velocity profiles (e.g., Appendix B of EPRI 2013). The randomization process introduces some smoothing of very sharp peaks computed using full resonance with deterministic profiles, but maintains fundamental resonances produced by pronounced changes in velocity with depth.

Randomization of the velocity profiles can be achieved through various processes. In general, the randomization can be partitioned into a model for the logarithmic standard deviation ($\sigma_{\ln Vs}$) and the correlation structure. EPRI (2013) used a generic standard deviation model of 0.25 at depths above 15 m and 0.15 below this depth. The Toro (1995) model, commonly applied at nuclear facilities, includes a depth-dependent correlation model that can be modified with both site-specific aleatory variability and correlation data. The challenge with the development of an aleatory model for any of the INL facility areas is that the complexity of the site conditions limits the ability to develop an aleatory variability model based on repeated measurements. Thus, the approach used in this study is to adopt a modification of the EPRI (2013) model for the aleatory variability of V_S and focus on the consideration of the epistemic uncertainty through alternative

19448201, 2026, 1, Downloaded from https://onlinelibrary.wiley.com/doi/10.1002/eqs4.70046 by Imperial College London, Wiley Online Library on [05/06/2026]. See the Terms and Conditions (https://onlinelibrary.wiley.com/terms-and-conditions) on Wiley Online Library for rules of use; OA articles are governed by the applicable Creative Commons License

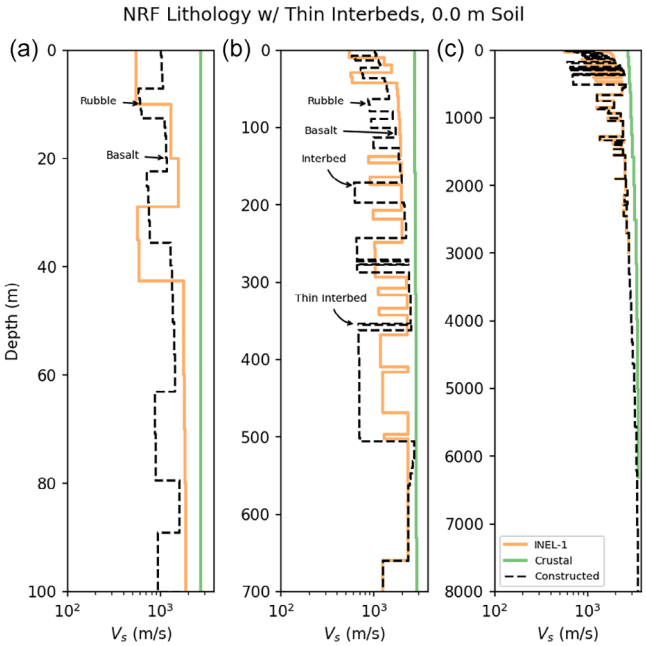

FIGURE 9 | Example construction of the NRF profile using lithology with stochastic thin interbeds, assuming 0 m of soil, illustrated over three depth ranges: (a) upper 100 m, (b) upper 700 m, and (c) the entire profile.

velocity models. The modification of the EPRI (2013) model refers to the randomization of MASW profiles, as explained in the next paragraph.

For the borehole- and SASW-based velocity profiles, a total of 60 randomized profiles were developed for each branch on the logic tree. The velocity profiles are randomized with $\sigma_{\ln Vs} = 0.2$ to a depth of 1 km, and $\sigma_{\ln Vs} = 0.1$ below this depth; for the near-surface soil, $\sigma_{\ln Vs} = 0.25$ is used if it is present in the profile. The value of $\sigma_{\ln Vs} = 0.2$ was selected to be consistent with the results of the mixture model (see Figure 7). For the MASW-based velocity profiles, multiple realizations were provided by Cox and Vantassel (2021) at each array location, and these profiles were used in lieu of profile randomization. The standard deviation from these model inversions is compared with the target model for NRF in Figure 10a. In some instances, the variation from the inversions is higher than the target, and in other cases, they are lower. To provide a more consistent variation in the randomized profile, the logarithmic standard deviation of the velocity randomization is reduced through a difference in variances such that the target aleatory variability is achieved through the combination of inversions and randomizations, defined by:

$$\sigma_{\ln Vs}^{\text{adjust}} = \sqrt{\max\left[\left(\sigma_{\ln Vs}^{\text{target}}\right)^2 - \left(\sigma_{\ln Vs}^{\text{inversion}}\right)^2, 0\right]} \tag{6}$$

In some instances, the inversion variation $\sigma_{\ln Vs}^{\text{inversion}}$ is much greater than the aleatory variability, and the target variation $\sigma_{\ln Vs}^{\text{target}}$ is exceeded; in these cases, the adjusted logarithmic standard deviation ($\sigma_{\ln Vs}^{\text{adjust}}$) is set to be zero, as shown in Figure 10b. This process results in 60 profiles, with each profile based on one of the 60 realizations from Cox and Vantassel (2021).

5.1 | Filtering of Surface-Wave Profiles

Griffiths et al. (2016) found that using the Toro (1995) randomization approach with a site-calibrated correlation structure led to velocity profiles that were inconsistent with the observed dispersion curve at a site. To address this potential shortcoming of the randomization, a novel process was developed to filter out (remove) randomized velocity profiles based on the dispersion curve, as recommended by Teague et al. (2018) and Hallal et al. (2022). The process involves first quantifying the uncertainty in dispersion curves, and then calculating a base-case profile specific target dispersion curve. Testing against measured dispersion curves would be preferable, but was not possible because measurements could not be collected for all site conditions. The filtering of the randomized profiles using the dispersion curves is intended to provide randomized velocity profiles that are more consistent with the uncertainty in the dispersion curves. The process does not add new information, but rather removes randomizations that are potentially inconsistent with a different perspective

19448201, 2026, 1, Downloaded from https://onlinelibrary.wiley.com/doi/10.1002/eqsp4.70046 by Imperial College London, Wiley Online Library on [05/06/2026]. See the Terms and Conditions (https://onlinelibrary.wiley.com/terms-and-conditions) on Wiley Online Library for rules of use; OA articles are governed by the applicable Creative Commons License

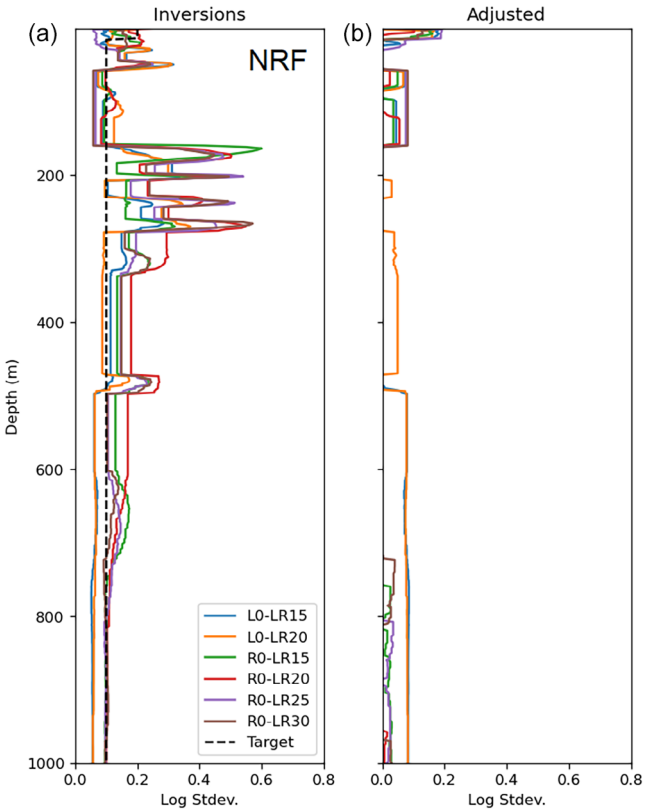

FIGURE 10 | (a) Logarithmic standard deviation $\sigma_{\ln V_S}$ from the MASW/MAM profiles at NRF, and (b) the adjusted logarithmic standard deviation for the randomization.

(i.e., dispersion curves vs. V_S profiles). For some base-case profiles, the filtering only impacts a few outlying profiles, while for other base-case profiles, many of the simulated profiles are rejected by the testing against the average dispersion curves. For details on the filtering of surface-wave profiles, please refer to Idaho National Laboratory (2022).

5.2 | Assignment of κ_0-Consistent Damping

Both the measured and randomized profiles have strong velocity reversals that have the potential to attenuate the high-frequency component of the ground motion. To provide profiles that are consistent with the target site attenuation parameter κ_0, the small-strain damping of the layers for each randomized profile is adjusted using the following approach.

In one-dimensional site response analysis, the total attenuation parameter ($\kappa_{0,\text{total}}$) comprises two primary components: small-strain material damping ($\kappa_{0,\text{damping}}$) and, to a lesser extent, scattering effects associated with wave propagation in the 1D profile ($\kappa_{0,\text{scatter}}$). The damping contribution required to achieve the target value of $\kappa_{0,\text{total}}$ for a given profile is expressed as:

$$\kappa_{0,\text{damping}} = \kappa_{0,\text{total}} - \kappa_{0,\text{scatter}} \tag{7}$$

The scattering term cannot be determined *a priori* because it depends on the velocity structure and the specific site response methodology. Consequently, $\kappa_{0,\text{scatter}}$ is estimated as the difference between the attenuation predicted from an assigned damping profile and the attenuation observed in the computed site transfer function. An initial damping configuration is adopted using representative values: 1% damping ($Q = 50$) in the upper 200 m and 0.33% damping ($Q = 152$) below 200 m depth. The acceleration transfer function between the half-space and the ground surface is then computed, and $\kappa_{0,\text{total}}$ is derived from the slope of the transfer function within the 50–200 Hz frequency range, following the procedure of Hough et al. (1988). The attenuation attributed to the prescribed damping is calculated using the formulation presented by Hough et al. (1988) and Silva and Darragh (1995):

$$\kappa_{0,\text{damping}} = \sum_{i}^{n} \frac{H(i)}{Q_S(i) V_S(i)} \tag{8}$$

19448201, 2026, 1, Downloaded from https://onlinelibrary.wiley.com/doi/10.1002/eqs4.70046 by Imperial College London, Wiley Online Library on [05/06/2026]. See the Terms and Conditions (https://onlinelibrary.wiley.com/terms-and-conditions) on Wiley Online Library for rules of use; OA articles are governed by the applicable Creative Commons License

here, V_S denotes the shear-wave velocity, Q_S is the shear-wave quality factor ($Q_S = 1/[2D]$, where D is the small-strain viscous damping ratio), and H is layer thickness. The computed $\kappa_{0,\text{total}}$ reflects the combined influence of damping and scattering, with the latter obtained as:

$$\kappa_{0,\text{scatter}} = \kappa_{0,\text{total}} - \kappa_{0,\text{damping}} \tag{9}$$

Once the $\kappa_{0,\text{scatter}}$ has been quantified, the damping contribution required to satisfy the target $\kappa_{0,\text{total}}$ can be calculated using Equation (7). The target value of κ_0 is discussed in the *Site Attenuation Parameters* section.

For a given $\kappa_{0,\text{damping}}$, the damping within each layer is defined using the following approach. Assuming that Q_S is proportional to V_S (Silva and Darragh 1995), then Equation (7) can be used to assign Q_S values to the layers in a crustal velocity profile, by computing the scale factor γ:

$$\gamma = \frac{\sum_i^n H(i)/V_{S(i)}^2}{\kappa_{0,\text{damping}}} \tag{10}$$

and then computing the V_S-proportional damping as:

$$D = \frac{1}{2\gamma V_S} \tag{11}$$

This process is repeated for all realizations from the randomization, because the randomization of the velocity profile requires that the small-strain damping for each realization is also different, such that $\kappa_{0,\text{total}}$ is consistent with the target value. The adjustment of the damping shifts the nonlinear curve up or down, as opposed to scaling the curve to the target value. This adjustment is focused on the small-strain damping behavior. Based on sensitivity studies performed by the GMC TI team, nonlinearity observed in the profiles is not significant, but approaches such as that of Xu and Rathje (2021) should be considered for applications for which nonlinearity is more significant.

5.3 | Averaging of Interbed Velocities

The final element to construct borehole-based velocity profiles is an approach to smooth the velocities of the interbeds. Such a smoothing was applied in previous studies at INL (Idaho National Laboratory 2016) to account for the limited extent of interbeds at INL sites. The GMC TI team performed sensitivity analyses to explore the impact of the thick interbeds at NRF. The sensitivity study consisted of running equivalent-linear site response analyses for a preliminary version of the best-estimate V_S profile along with two alternative profiles: one where the interbeds were removed (upper-bound profile), and another where the upper 700 m of the profile were assigned the V_S model for the interbeds (lower-bound profile). The analyses illustrated that the presence of the interbeds leads to significantly lower amplitudes compared to a site without interbeds. By comparing empirical transfer functions at a nearby seismic station (NVRF), we found that the best-estimate profile at NRF overestimates the amount of attenuation and would lead to an underestimate of ground shaking. For this reason, the site response logic tree includes alternatives for smoothing the low-velocity interbeds.

Two approaches were investigated for smoothing the low-velocity layers: (1) the application of smoothing windows of different widths to the velocity profile, and (2) the assignment of an effective velocity to the interbed that is an average of the interbed velocity and that of the adjacent layers (essentially presuming that some wave passage occurs through the edges of laterally-discontinuous interbeds). The smoothing-window approach results in a smoothly varying velocity with depth, while the effective-velocity approach preserves the sharp velocity contrasts that are observed at the location of sedimentary interbeds, as seen in Figure 11a. Sensitivity studies using linear-elastic site response showed that although both approaches reduced the large attenuation observed for the profile with interbeds, they resulted in different strains in the interbeds, with the smoothing-window approach resulting in higher strains.

The GMC TI team opted for the effective-velocity approach because the sharp velocity contrasts at the location of the interbeds are a feature that is clearly seen in velocity logs measured with suspension logging (Figure 3). Moreover, the 2D site response analyses conducted by Asimaki (2021) indicated that the strains in 2D site response analyses were lower than those in 1D analyses, thus indicating that the reduced strains observed in the effective velocity approach are consistent with non-1D effects. The Asimaki (2021) study found that the velocity structure introduced a bias in 1D analysis at one target location (nor NRF). Ultimately, the bias was incorporated into the site adjustment factor for the affected target location as an additional level to the site response logic tree.

19448201, 2026, 1, Downloaded from https://onlinelibrary.wiley.com/doi/10.1002/eqs4.70046 by Imperial College London, Wiley Online Library on [05/06/2026]. See the Terms and Conditions (https://onlinelibrary.wiley.com/terms-and-conditions) on Wiley Online Library for rules of use; OA articles are governed by the applicable Creative Commons License

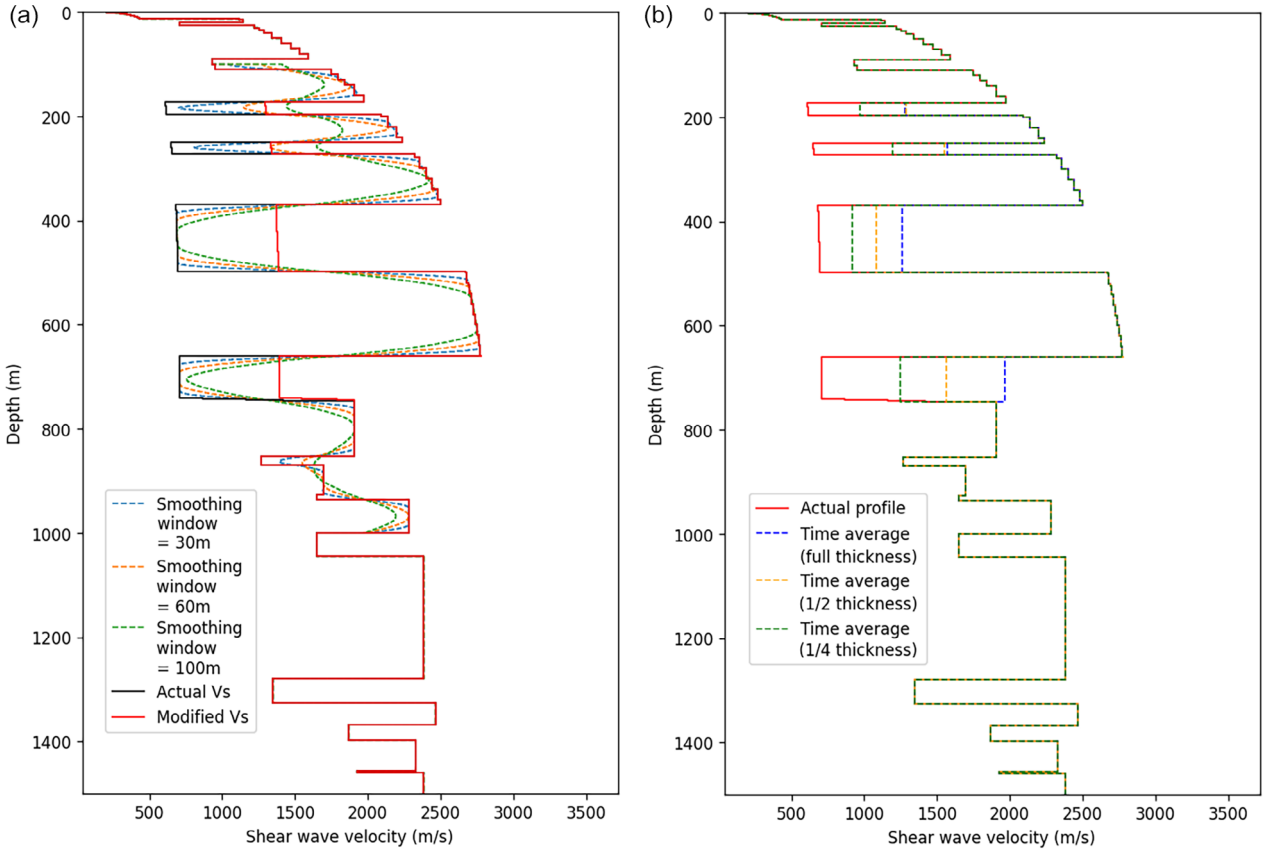

FIGURE 11 | Shear-wave velocity profiles corresponding to: (a) the smoothing approach versus the effective-velocity approach for addressing the low-velocity layers (the "Modified V_S" profile is obtained using the effective velocity approach with 1/2 thickness, as seen in the figure on the right); and (b) alternative averaging windows for the effective velocity approach that entered the site response logic-tree.

The approach adopted to select an effective velocity was to obtain the travel-time-averaged V_S of the interbed along with a portion of the adjacent basalt layers. Several average window widths were considered: full, half, or a quarter of the thickness of surrounding basalt layers (Figure 11b). We found that as the thickness of the surrounding basalt layer increases, the impacts of the interbeds are reduced (i.e., less attenuation in the interbeds). However, there is not much difference between using half- or full-width of the neighboring basalt layers (see Figures 11–35 of Idaho National Laboratory 2022). The GMC TI team opted to select the options with the half- and quarter-width of the surrounding basalt, as these provide distinct options for smoothing. In the site response logic-tree (Figure 5), a higher weight (0.6) was assigned to the smoothing incorporating half of the surrounding basalt layers, because this results in stronger smoothing and is more consistent with the empirical transfer function. A low (0.1) weight is given to the no-averaging option to reflect the possibility that the low-velocity zones are continuous across the sites. The remaining option (smoothing option with a quarter of the adjacent basalt layers) is given the balance of the weight (0.3).

6 | Hazard-Consistent Input Motions

In the one-step approach, the SAFs represent the relative site response of the target site profiles compared to that of the host reference rock profile to the same input motion at depth. These representative motions were developed using the conditional mean spectra (CMS) concept (Baker and Cornell 2006; Baker 2011). The CMS approach was chosen instead of scaling median spectral shapes (e.g., EPRI 2013) because CMS represent more realistic scenario response spectra at high ground-motion levels compared to the upward scaling of median spectral shapes to match specified ground-motion levels at particular periods (Carlton and Abrahamson 2014). Defining the site amplification functions requires CMS motions that capture the entire period range of interest (i.e., 0.01–10 s). To reduce the number of CMS required, the CMS were broadened based on the Kishida (2017) approach and used to define CMS over three period ranges: (1) a short-period range of PGA to 0.1 s, (2) an intermediate-period range of 0.15–1.0 s, and (3) a long-period range of 1.5–10.0 s. As the

19448201, 2026, 1, Downloaded from https://onlinelibrary.wiley.com/doi/10.1002/eqs4.70046 by Imperial College London, Wiley Online Library on [05/06/2026]. See the Terms and Conditions (https://onlinelibrary.wiley.com/terms-and-conditions) on Wiley Online Library for rules of use; OA articles are governed by the applicable Creative Commons License

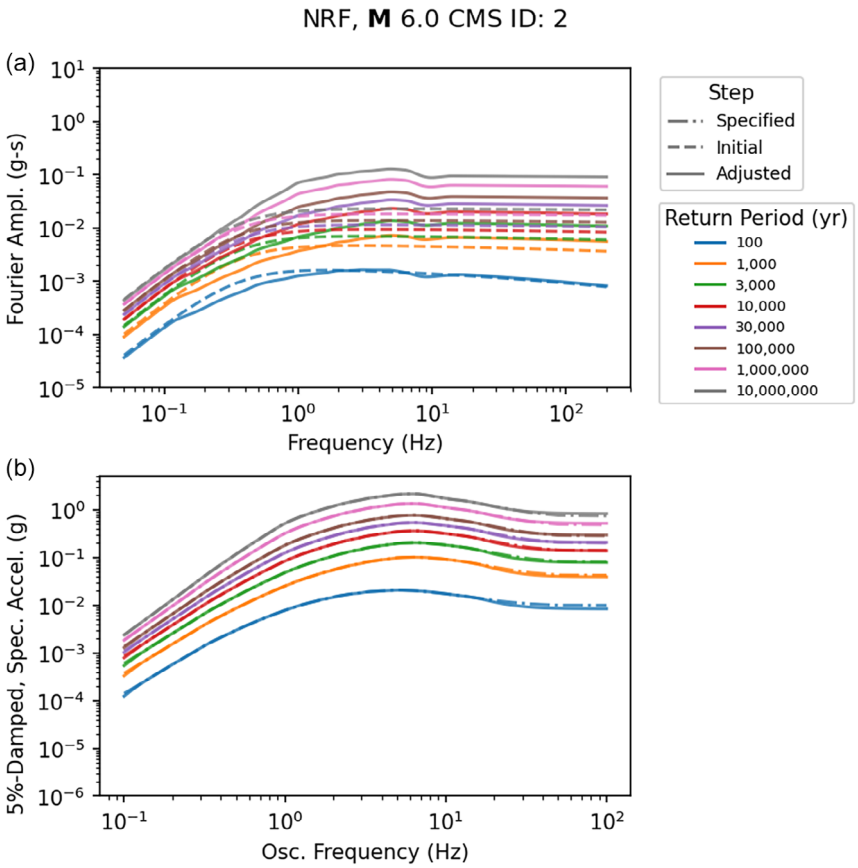

FIGURE 12 | Example CMS input motions for the NRF facility area: (a) Initial and adjusted FAS, and (b) specified and adjusted response spectra. The target periods for the CMS are the intermediate period range (0.15–1.0 s).

number of period ranges increases, the CMS become more narrow-banded, and thus more realistic, at the cost of increased calculation time.

The CMS motions are defined at the surface of the host profile and then modified to be consistent with the base of the profile (a process commonly known as deconvolution). In place of traditional time-domain deconvolution, we adopted an approach similar to the Rathje et al. (2005) methodology. An initial FAS without any site effects is defined at the base of the profile using Stafford et al. (2022) and then modified to be consistent with the specified response spectrum at the surface of the host profile. In this approach, a correction factor is determined using the misfit of the response spectrum computed at the surface relative to the specified motion. This correction factor is applied to the FAS at the base of the profile, modifying it to be consistent with the specified response spectrum at the surface. The advantages of this process are that it starts with a realistic Fourier amplitude spectrum shape and avoids the deconvolution, which has the potential to result in unrealistic distortions.

Examples of the initial and adjusted FAS and the specified and adjusted response spectra are shown in Figure 12. Note that the specified and adjusted response spectra are so similar at some periods that they are indistinguishable. Differences between the initial and adjusted FAS depend on the return period. As the return period lengthens, the specified response spectra deviate more from a median shape, thus the compatible FAS requires greater adjustment. The resulting response spectra compare well with the specified spectra, with some minor discrepancies above 20 Hz.

7 | Results of Site Adjustment Factors

The site response simulations were performed using the Python package *pystrata* (Kottke and Millen 2023) on Amazon Web Services Fargate to run 1,000 instances simultaneously. Use of this cloud infrastructure permitted accommodating the large number of simulations required to sample the logic tree, randomized profiles, and CMS input motions. For the NRF facility area, this required 907,200 site response simulations, and for all INL sites and hazard targets, 18,184,320 simulations were performed.

19448201, 2026, 1, Downloaded from https://onlinelibrary.wiley.com/doi/10.1002/eqsp4.70046 by Imperial College London, Wiley Online Library on [05/06/2026]. See the Terms and Conditions (https://onlinelibrary.wiley.com/terms-and-conditions) on Wiley Online Library for rules of use; OA articles are governed by the applicable Creative Commons License

Example results of the computation of SAFs for the NRF facility area are shown in Figure 13. The sampling of the SAFs is conducted following the guidelines given in Rodriguez-Marek, Rathje, et al. (2021). As described therein, a minimum epistemic uncertainty is imposed on the distribution of SAFs. The value selected for the minimum epistemic uncertainty was selected to be 0.2 by the TI Team (for details, see Idaho National Laboratory 2022). This selected minimum epistemic uncertainty is lower than that suggested by studies utilizing borehole data (e.g., Stewart and Afshari 2021; Pretell et al. 2023) but is consistent with, or slightly higher than, values used in similar projects in the past (e.g., the Thyspunt Nuclear Siting Project; Rodriguez-Marek et al. 2014). Model error estimates from downhole arrays are likely affected by pseudoresonances. Site response for downhole arrays defines the input motion as a "within" motion with both up- and down-going waves, which produce strong pseudoresonances in the profile (Tao and Rathje 2020), whereas the site response analysis performed in this study uses a complete site column with an outcrop, which is not sensitive to these pseudoresonances.

The sampling of SAFs is repeated for different magnitudes to capture dependence on magnitude (Stafford et al. 2017) and input motion intensities and to capture the impact of material nonlinearity (Figure 14). The contribution of different branches of the logic tree to the overall epistemic uncertainty is illustrated via tornado plots in Figure 15. As expected, Figure 15 indicates that the uncertainty in site kappa dominates the epistemic uncertainty in site adjustment factors at high frequencies. For intermediate and low frequencies, the uncertainty in the SAF is dominated by the uncertainty in the profile. The V_S averaging branch, which corresponds to the choice of averaging method for interbeds, contributes to high-frequency attenuation and shows up as a contributor at 5 Hz, though not at 100 Hz. Not surprisingly, the lowest contributor to uncertainty is the MRD curves; this is due to the relatively low strains observed in the profiles.

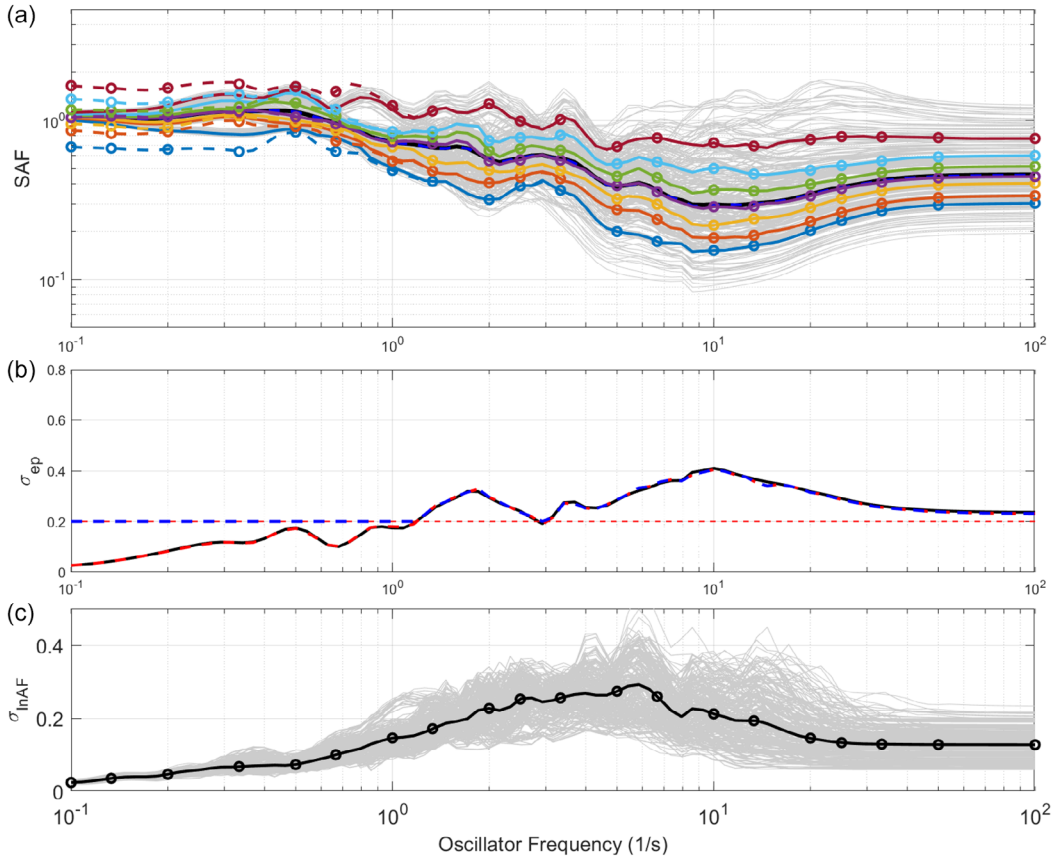

FIGURE 13 | Example of the process to obtain sample SAFs (shown here for **M** 7.0, 10,000-yr return period, and no soil cover). (a) Thin gray lines are the average response for each terminal branch of the logic tree; the solid-colored lines are the seven sampled SAFs, the dashed lines take into consideration minimum epistemic uncertainty, and the markers correspond to the periods sampled for hazard. (b) The black line is the epistemic uncertainty in the site response logic-tree, the dashed thick red line is the epistemic uncertainty computed from the sampled SAFs, and the dashed blue line is the epistemic uncertainty of the modified sampled SAF (modified to account for minimum epistemic uncertainty, shown as thin red dashed lines). (c) Thin lines are the aleatory variability for each branch of the logic tree, and the thick black line is the weighted average aleatory variability.

19448201, 2026, 1, Downloaded from https://onlinelibrary.wiley.com/doi/10.1002/eqs4.70046 by Imperial College London, Wiley Online Library on [05/06/2026]. See the Terms and Conditions (https://onlinelibrary.wiley.com/terms-and-conditions) on Wiley Online Library for rules of use; OA articles are governed by the applicable Creative Commons License

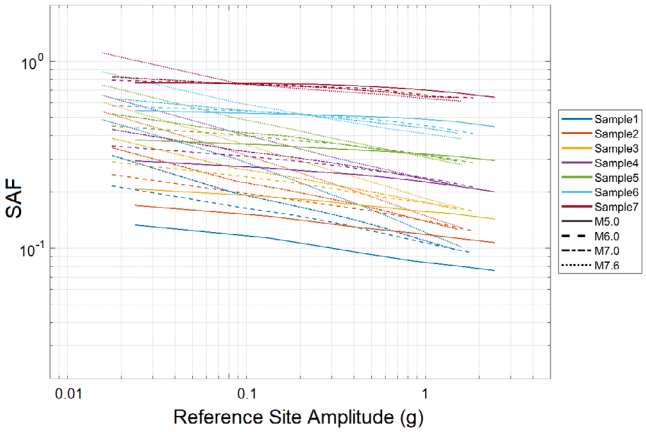

FIGURE 14 | Sampled SAFs for hazard calculation for the NRF site and no soil cover, for a selected oscillator period ($T = 0.1$ s). Each sample (Sample1, Sample2, etc.) refers to downsampling from the full site response logic tree (see section on *Site Response Logic-Tree Approach*).

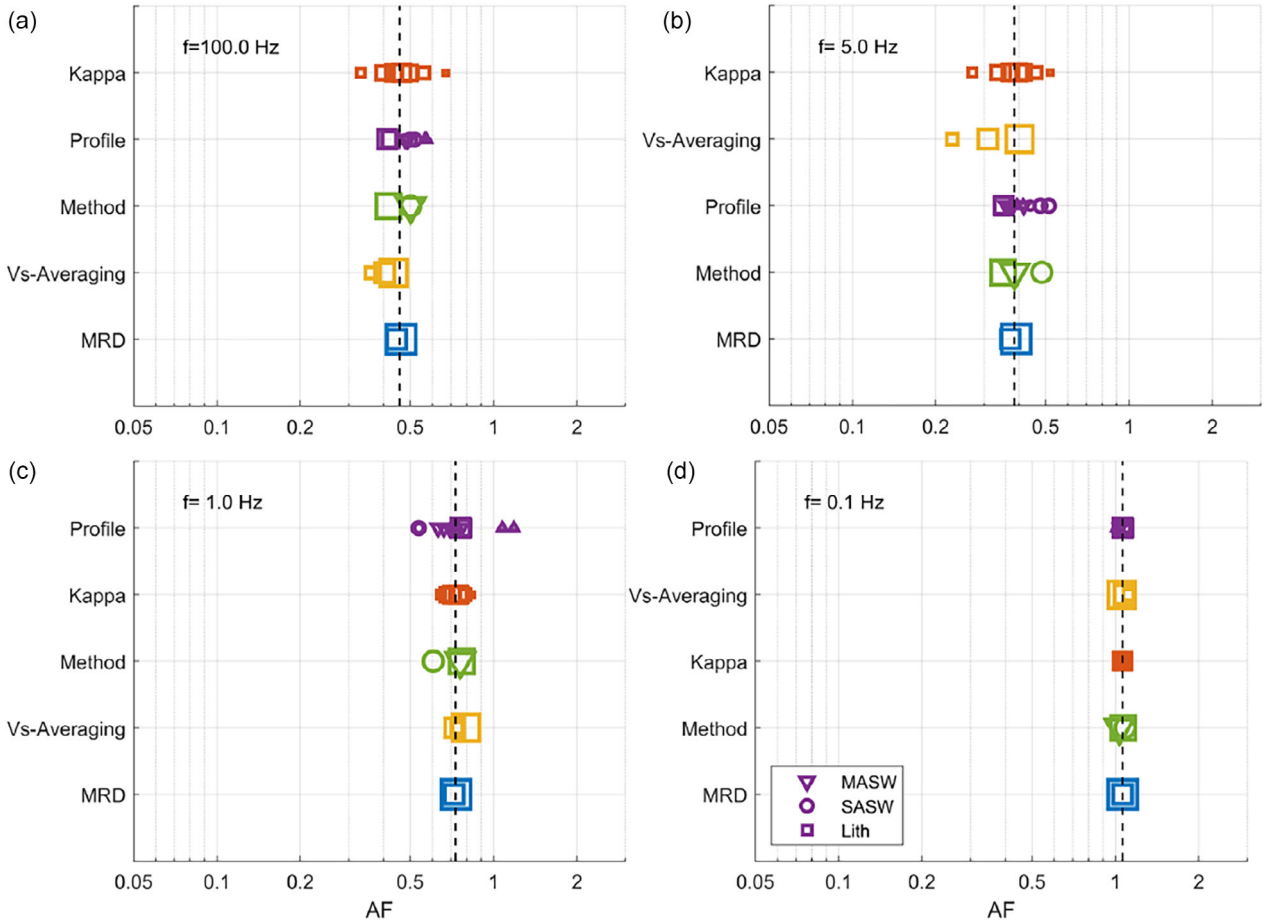

FIGURE 15 | Tornado plots for **M** 7.0 and for input ground motions consistent with a 10,000-year return period. Plots are shown for selected oscillator frequencies: (a) 100 Hz, (b) 5 Hz, (c) 1 Hz, and (d) 0.1 Hz. Tornado plots illustrate the conditional mean for each branch of the logic tree within each logic tree node (i.e., the value of the SAF if that branch was the only branch for that logic tree node). Marker size is proportional to the weight of each branch. The vertical dashed line is the mean value of the SAF.

8 | Conclusions

The implementation of host-to-target site adjustment in a full probabilistic seismic hazard assessment requires that the site adjustment factors fully capture the epistemic uncertainty in the adjustment. In this paper, we presented an application of host-to-target site adjustments for the SSHAC Level 3 PSHA conducted for Idaho National Laboratory.

19448201, 2026, 1, Downloaded from https://onlinelibrary.wiley.com/doi/10.1002/eqs4.70046 by Imperial College London, Wiley Online Library on [05/06/2026]. See the Terms and Conditions (https://onlinelibrary.wiley.com/terms-and-conditions) on Wiley Online Library for rules of use; OA articles are governed by the applicable Creative Commons License

This implementation uses the one-step correction approach along with site response logic trees. Key to this approach is that site response analyses are conducted for each end-branch of the logic tree, and the resulting SAFs are then sampled via a discrete distribution. This methodology ensures that the epistemic uncertainty is appropriately captured in ground-motion space (Atkinson et al. 2014; Rodriguez-Marek, Bommer, et al. 2021; Rodriguez-Marek, Rathje, et al. 2021).

The implementation of the host-to-target approach to the INL PSHA demonstrated the importance of collecting site data using multiple complementary measurement techniques. These include, in addition to alternative methods for measuring the V_S profile at the site, the incorporation of geotechnical and geological information to construct site profiles, and the use of surface-wave dispersion curves to constrain profile randomization such that the resulting randomized profiles are consistent with measured dispersion curves at a site. The site response logic-tree approach then allows for the incorporation of all sources of data, leading to a proper capture of epistemic uncertainty.

This study also demonstrated the tremendous importance of recordings to reduce epistemic uncertainty. In particular, the availability of recordings at the site allowed for reducing the uncertainty in the target site kappa (κ_0) distribution. Moreover, recordings at ground-motion stations in the INL footprint were used to help assign weights to alternative logic tree branches and to constrain approaches for smoothing velocity profiles, such that the impact of low-velocity interbeds is consistent with observed ground motions. The importance of instrumenting critical facilities is highlighted by the fact that small-magnitude earthquakes were useful to constrain the model for hazard-significant events. Instrumenting a site in the early stages of project development can thus render useful data within project schedule constraints.

The implementation of the one-step approach for host-to-target adjustment of site effects was presented in this study. Although some aspects of the logic tree are unique to the geologic conditions encountered at INL and similar geologic environments (e.g., dealing with interbedded layers of sediment within rock), the one-step host-to-target site adjustment approach is intended to be broadly applicable and adaptable. Together with the Boore et al. (2022) and Boore (2023) approach for host-to-target source and path adjustments, this methodology provides a framework for site-specific PSHA that can be easily adapted to other studies.

Acknowledgments

The authors would like to acknowledge all participants and sponsors of the Idaho National Laboratory SSHAC Level 3 PSHA project, including INL project managers Sam Dixon and Josh Jacobson. The development of the GMC model was greatly enhanced by constructive reviews from the project Participatory Peer Review Panel, consisting of Marty McCann, Richard Lee, Richard Quittmeyer, Ellen Rathje, and Dick Smith. The authors are also grateful to the numerous specialty contractors who contributed to the GMC model, including Brady Cox, Joe Vantassel, Kenneth Stokoe, Rob Steller, John Diehl, Domniki Asimaki, Bob Darragh, Walt Silva, Tadahiro Kishida, and Olga-Joan Ktenidou. In addition, the authors would like to acknowledge reviews of this paper by Gabriele Ameri, Brady Cox, and an anonymous reviewer, whose feedback improved the quality of this paper.

Conflicts of Interest

The authors declare no conflicts of interest.

Data Availability Statement

The project site characterization and ground motion data are unavailable. The software used to perform the site response analyses is a Python-based site response library, pyStrata (Kottke and Millen 2023), and available on Github: https://github.com/arkottke/pystrata. pyStrata was run in Docker containers on Amazon Web Services, configured using Terraform scripts and available on Github (Kottke and Hearn 2024): https://github.com/arkottke/docker-pystrata. The dispersion curves were computed using geopsy (Wathelet et al. 2020).

References

Abrahamson, N. A., W. J. Silva, and R. Kamai. 2014. "Summary of the ASK14 Ground Motion Relation for Active Crustal Regions." *Earthquake Spectra* 30, no. 3: 1025–1055.

Al Atik, L., and N. Abrahamson. 2021. "A Methodology for the Development of 1D Reference V_S Profiles Compatible with Ground-Motion Prediction Equations: Application to NGA-West2 GMPEs." *Bulletin of the Seismological Society of America* 111, no. 4: 1765–1783.

Asimaki, D. 2021. *Evaluation of Two-Dimensional to One-Dimensional Site Response for the Idaho National Laboratory*. Battelle Energy Alliance External Report INL/EXT-21-62288. 43.

19448201, 2026, 1, Downloaded from https://onlinelibrary.wiley.com/doi/10.1002/eqs4.70046 by Imperial College London, Wiley Online Library on [05/06/2026]. See the Terms and Conditions (https://onlinelibrary.wiley.com/terms-and-conditions) on Wiley Online Library for rules of use; OA articles are governed by the applicable Creative Commons License

Atkinson, G. M., J. J. Bommer, and N. A. Abrahamson. 2014. "Alternative Approaches to Modeling Epistemic Uncertainty in Ground Motions in Probabilistic Seismic-Hazard Analysis." *Seismological Research Letters* 85, no. 6: 1141–1144.

Baker, J. 2011. "Conditional Mean Spectrum: Tool for Ground Motion Selection." *Journal of Structural Engineering* 137: 322–331.

Baker, J., and C. Cornell. 2006. "Spectral Shape, Epsilon and Record Selection." *Earthquake Engineering and Structural Dynamics* 35: 1077–1095.

Bommer, J. J. 2012. "Challenges of Building Logic Trees for Probabilistic Seismic Hazard Analysis." *Earthquake Spectra* 28, no. 4: 1723–1735.

Bommer, J. J. 2022. "Earthquake Hazard and Risk Analysis for Natural and Induced Seismicity: Towards Objective Assessments in the Face of Uncertainty." *Bulletin of Earthquake Engineering* 20, no. 6: 2825–3069.

Bommer, J. J., and P. J. Stafford. 2020. "Selecting Ground-Motion Models for Site-Specific PSHA: Adaptability versus Applicability." *Bulletin of the Seismological Society of America* 110, no. 6: 2801–2815.

Boore, D. M., J. P. Stewart, E. Seyhan, and G. M. Atkinson. 2014. "NGA-West2 Equations for Predicting PGA, PGV, and 5% Damped PSA for Shallow Crustal Earthquakes." *Earthquake Spectra* 30, no. 3: 1057–1085.

Boore, D. M., R. R. Youngs, A. R. Kottke, et al. 2022. "Construction of a Ground-Motion Logic Tree through Host-to-Target Region Adjustments Applied to an Adaptable Ground-Motion Prediction Model." *Bulletin of the Seismological Society of America* 112, no. 6: 3063–3080.

Boore, D. M. 2003. "Simulation of Ground Motion Using the Stochastic Method." *Pure and Applied Geophysics* 160: 635–676.

Boore, D. M. 2016. "Determining Generic Velocity and Density Models for Crustal Amplification Calculations, with an Update of the Boore and Joyner (1997) Generic Site Amplification for $\overline{V}_S(Z) = 760$ m/s." *Bulletin of the Seismological Society of America* 106, no. 1: 313–317.

Boore, D. M. 2023. "Construction of a Ground-Motion Logic Tree through Host-to-Target Region Adjustments Applied to an Adaptable Ground-Motion Prediction Model: An Addendum." *Bulletin of the Seismological Society of America* 114, no. 2: 1003–1014.

Bozorgnia, Y., N. A. Abrahamson, L. Al Atik, et al. 2014. "NGA-West2 Research Project." *Earthquake Spectra* 30, no. 3: 973–987.

Campbell, K. W., and Y. Bozorgnia. 2014. "NGA-West2 Ground Motion Model for the Average Horizontal Components of PGA, PGV, and 5% Damped Linear Acceleration Response Spectra." *Earthquake Spectra* 30, no. 3: 1087–1115.

Carlton, B., and N. A. Abrahamson. 2014. "Issues and Approaches for Implementing Conditional Mean Spectra in Practice." *Bulletin of the Seismological Society of America* 104: 503–512.

Chiou, B. S.-J., and R. R. Youngs. 2014. "Update of the Chiou and Youngs NGA Model for the Average Horizontal Component of Peak Ground Motion and Response Spectra." *Earthquake Spectra* 30, no. 3: 1117–1153.

Cox, B. R., and D. P. Teague. 2016. "Layering Ratios: A Systematic Approach to the Inversion of Surface Wave Data in the Absence of a-Priori Information." *Geophysical Journal International* 207: 422–438.

Cox, B. R., and J. P. Vantassel. 2021. *Deep Shear Wave Velocity Profiling Using MASW and MAM Surface Seismic Techniques*. Battelle Energy Alliance External Report INL/EXT-21–62823. 286.

Darendeli, M. B. 2001. "*Development of a New Family of Normalized Modulus Reduction and Material Damping Curves*." *Ph.D. Dissertation*, University of Texas at Austin. 395.

Electric Power Research Institute [EPRI]. 2013. *Seismic Evaluation Guidance: Screening, Prioritization and Implementation Details (SPID) for the resolution of Fukushima Near-Term Task Force Recommendation 2.1: Seismic*. Final Report. Electric Power Research Institute.

Griffiths, S. C., B. R. Cox, E. M. Rathje, and D. P. Teague. 2016. "Surface-Wave Dispersion Approach for Evaluating Statistical Models that Account for Shear-Wave Velocity Uncertainty." *Journal of Geotechnical and Geoenvironmental Engineering* 142: 04016061.

Hallal, M. M., and B. R. Cox. 2021. "An H/V Geostatistical Approach for Building Pseudo-3D *V*s Models to Account for Spatial Variability in Ground Response Analyses Part II: Application to 1D Analyses at Two Downhole Array Sites." *Earthquake Spectra* 37, no. 3: 1931–1954.

Hallal, M. M., and B. R. Cox. 2023. "What Spatial Area Influences Seismic Site Response: Insights Gained from Multiazimuthal 2D Ground Response Analyses at the Treasure Island Downhole Array." *Journal of Geotechnical and Geoenvironmental Engineering* 149, no. 1: 04022124.

Hallal, M. M., B. R. Cox, and J. P. Vantassel. 2022. "Comparison of State-of-the-Art Approaches Used to Account for Spatial Variability in 1D Ground Response Analyses." *Journal of Geotechnical and Geoenvironmental Engineering* 148, no. 5: 04022019.

Hardin, B. O., and F. E. Richart Jr. 1963. "Elastic Wave Velocities in Granular Soil." *Journal of the Soil Mechanics and Foundations Division* 89, no. 1: 33–65.

19448201, 2026, 1, Downloaded from https://onlinelibrary.wiley.com/doi/10.1002/eqs4.70046 by Imperial College London, Wiley Online Library on [05/06/2026]. See the Terms and Conditions (https://onlinelibrary.wiley.com/terms-and-conditions) on Wiley Online Library for rules of use; OA articles are governed by the applicable Creative Commons License

Hassani, B., G. M. Atkinson, M. Fairhurst, L. Yan, J. P. Stewart, and M. Sheffer. 2025. "Non-Ergodic Correction Factors for Hard Rock Sites in Western Canada, *Earthquake Spectra* 41, no. 2: 1060–1093.

Hough, S. E., J. G. Anderson, J. Brune, et al. 1988. "Attenuation near Anza, California." *Bulletin of the Seismological Society of America* 78, no. 2: 672–691.

Idaho National Laboratory. 2016. *SSHAC Level 1 Probabilistic Seismic Hazard Analysis for the Idaho National Laboratory*. Battelle Energy Alliance External Report INL/EXT-15-36682. Revision 2. 573.

Idaho National Laboratory. 2022. *Idaho National Laboratory Sitewide SSHAC Level 3 Probabilistic Seismic Hazard Analysis*. Battelle Energy Alliance Report No. INL/RPT-22-70233. 2487. Accessed November 2025. https://inldigitallibrary.inl.gov/PRR/INL-RPT-22-70233.pdf.

Kishida, T. 2017. "Conditional Mean Spectra Given a Vector of Spectral Accelerations at Multiple Periods." *Earthquake Spectra* 33: 469–479.

Kottke, A. R., and M. Millen. 2023. *Arkottke/Pystrata (v0.5.2)*. Zenodo. https://doi.org/10.5281/zenodo.7551992.

Kottke, A. R., and B. Hearn. 2024. *Arkottke/Docker-Pystrata (v0.1.0)*. Zenodo. https://doi.org/10.5281/zenodo.12533417.

Mavko, G., and T. Vanorio. 2010. "The Influence of Pore Fluids and Frequency on Apparent Effective Stress Behavior of Seismic Velocities." *Geophysics* 75, no. 1: N1–N7.

McLing, T., M. McCurry, C. Cannon, et al. 2014. "David Blackwell's Forty Years in the Idaho Desert, the Foundation for 21st Century Geothermal Research." *Geothermal Resources Council Transactions* 38: 143–153.

Menq, F. Y. 2003. "*Dynamic Properties of Sandy and Gravelly Soils*." *Ph.D. Dissertation*, University of Texas at Austin. 390.

Miller A. C. III, and T. R. Rice. 1983. "Discrete Approximations of Probability Distributions." *Management Science* 29: 352–362.

North Wind Resource Consulting, LLC, and Rizzo Associates. 2015. *Geotechnical Report, Spent Fuel Handling Recapitalization Project, Naval Reactors Facility, Idaho National Laboratory*. Prepared for Naval Reactors Facility, Bechtel Marine Propulsion Corporation. 130 with Appendix A-J.

Payne, S. J., B. D. Coryell, and J. M. Hubbell. 2012. *Evaluations of Existing Subsurface Data and Recommendations for New Data Collection in Support of INL Probabilistic Seismic Hazard Analysis*. Battelle Energy Alliance External Report INL/LTD-12-26965. Revision 0. 174.

Pretell, R., N. A. Abrahamson, and K. Ziotopoulou. 2023. "A Borehole Array Data–based Approach for Conducting 1D Site Response Analyses II: Accounting for Modeling Errors." *Earthquake Spectra* 39, no. 3: 1502–1533.

Rathje, E. M., A. R. Kottke, and M. C. Ozbey. 2005. "Using Inverse Random Vibration Theory to Develop Input Fourier Amplitude Spectra for Use in Site Response." In *16th International Conference on Soil Mechanics and Geotechnical Engineering, TC4 Earthquake Geotechnical Engineering Satellite Conference*. 160–166.

Richins, W. D., J. C. Pechmann, R. B. Smith, et al. 1987. "The 1983 Borah Peak, Idaho Earthquake and Its Aftershocks." *Bulletin of the Seismological Society of America* 77: 694–723.

Rizzo Associates Inc. 1994. *Geophysical Testing Program Expended Core Facility. INEL*. Report Prepared for Naval Reactors Facility. Project Number 93-1350. 32.

Rizzo Associates, Inc. 2008. *Field Investigation for Geotechnical and Geophysical Data Collection and Analysis: Comprehensive ECF Water Pit Seismic Evaluation*. Report Prepared for Naval Reactors Facility. Project Number 93-1350. 242.

Rodriguez-Marek, A., E. M. Rathje, J. J. Bommer, F. Scherbaum, and P. J. Stafford. 2014. "Application of Single-Station Sigma and Site-Response Characterization in a Probabilistic Seismic-Hazard Analysis for a New Nuclear Site." *Bulletin of the Seismological Society of America* 104, no. 4: 1601–1619.

Rodriguez-Marek, A., J. J. Bommer, R. R. Youngs, M. J. Crespo, P. J. Stafford, and M. Bahrampouri. 2021. "Capturing Epistemic Uncertainty in Site Response." *Earthquake Spectra* 37, no. 2: 921–936.

Rodriguez-Marek, A., E. Rathje, J. Ake, et al. 2021. "*Documentation Report for SSHAC Level 2: Site Response*." Office of Nuclear Regulatory Research, *Research Information Letter RIL2021-15*. 217. https://www.nrc.gov/docs/ML2132/ML21323A056.pdf.

Salvatier, J., T. V. Wiecki, and C. Fonnesbeck. 2016. "Probabilistic Programming in Python Using PyMC3." *PeerJ Computer Science* 2: e55.

Silva, W., and B. Darragh. 1995. *Engineering Characterization of Strong Ground Motion Recorded at Rock Sites*. Electric Power Research Institute Report No. TR-102262.

Silva, W., B. Darragh, T. Kishida, O. Ktenidou, and E. Pikoulis. 2021. *INL SSHAC Level 3 Study: Estimation of Source, Path, and Site Parameters and Their Uncertainty*. Battelle Energy Alliance External Report INL/EXT-21–65281. 266.

Stafford, P. J., D. M. Boore, R. R. Youngs, and J. J. Bommer. 2022. "Host-Region Parameters for an Adjustable Model for Crustal Earthquakes to Facilitate the Implementation of the Backbone Approach to Building Ground-Motion Logic Trees in Probabilistic Seismic Hazard Analysis." *Earthquake Spectra* 38, no. 2: 917–949.

19448201, 2026, 1, Downloaded from https://onlinelibrary.wiley.com/doi/10.1002/eqs4.70046 by Imperial College London, Wiley Online Library on [05/06/2026]. See the Terms and Conditions (https://onlinelibrary.wiley.com/terms-and-conditions) on Wiley Online Library for rules of use; OA articles are governed by the applicable Creative Commons License

Stafford, P. J., A. Rodriguez-Marek, B. Edwards, P. P. Kruiver, and J. J. Bommer. 2017. "Scenario Dependence of Linear Site-Effect Factors for Short-Period Response Spectral Ordinates." *Bulletin of the Seismological Society of America* 107: 2859–2872.

Stewart, J. P., and K. Afshari. 2021. "Epistemic Uncertainty in Site Response as Derived from One- Dimensional Ground Response Analyses." *Journal of Geotechnical and Geoenvironmental Engineering* 147, no. 1: 04020146.

STRATA Inc. 2011. *Final Report, Geotechnical Engineering Evaluation, Spent Fuel Handling Project Facility, Naval Reactors Facility - INL, Butte County, Idaho*. Prepared for Michael Baker Jr. Inc. 56.

Tao, Y., and E. Rathje. 2020. "Taxonomy for Evaluating the Site-Specific Applicability of One-Dimensional Ground Response Analysis." *Soil Dynamics and Earthquake Engineering* 128: 105865.

Teague, D. P., B. R. Cox, and E. M. Rathje. 2018. "Measured vs. Predicted Site Response at the Garner Valley Downhole Array considering Shear Wave Velocity Uncertainty from Borehole and Surface Wave Methods." *Soil Dynamics and Earthquake Engineering* 113: 339–355.

Toro, G. R. 1995. *Probabilistic Models of Site Velocity Profiles for Generic and Site-Specific Ground Motion Amplification Studies*. Department of Nuclear Energy, Brookhaven National Laboratory.

US Nuclear Regulatory Commission [USNRC]. 2018. Implementation Guidelines for SSHAC Hazard Studies. *NUREG-2213*. US Nuclear Regulatory Commission.

Wang, Y., and K. H. Stokoe. 2022. "Development of Constitutive Models for Linear and Nonlinear Shear Modulus and Material Damping Ratio of Uncemented Soils." *Journal of Geotechnical and Geoenvironmental Engineering* 148: 04021192.

Wathelet, M., J. L. Chatelain, C. Cornou, et al. 2020. "Geopsy: A User-Friendly Open-Source Tool Set for Ambient Vibration Processing." *Seismological Research Letters* 91: 1878–1889.

Whitehead, R. L. 1992. *Geohydrologic Framework of the Snake River Plain Regional Aquifer System, Idaho and Eastern Oregon*. U.S. Geological Survey Professional Paper No. 1408-B. U.S. Government Printing Office.

Williams, T., and N. Abrahamson. 2021. "Site-Response Analysis Using the Shear-Wave Velocity Profile Correction Approach." *Bulletin of the Seismological Society of America* 111, no. 4: 1989–2004.

Wood Environment & Infrastructure Solutions, Inc. 2021a. *Seismic Velocity Borehole Report for Naval Reactors Facility (NRF) at INL*. Battelle Energy Alliance External Report INL/EXT-21-62337. 703.

Wood Environment & Infrastructure Solutions, Inc. 2021b. *Final Study Report: Idaho National Laboratory Spectral Analysis of Surface Waves Testing*. Battelle Energy Alliance External Report INL/EXT-21-65012. 150.

Wood Environment & Infrastructure Solutions, Inc. and University of Texas at Austin. 2022. *Laboratory Testing of Sedimentary Interbed and Basalt Cores from INL Seismic Velocity Boreholes*. Battelle Energy Alliance Report INL/RPT-22-66692. 866.

Xu, B., and E. M. Rathje. 2021. "The Effect of Soil Nonlinearity on High-Frequency Spectral Decay and Implications for Site Response Analysis." *Earthquake Spectra* 37: 686–706.

19448201, 2026, 1, Downloaded from https://onlinelibrary.wiley.com/doi/10.1002/eqs4.70046 by Imperial College London, Wiley Online Library on [05/06/2026]. See the Terms and Conditions (https://onlinelibrary.wiley.com/terms-and-conditions) on Wiley Online Library for rules of use; OA articles are governed by the applicable Creative Commons License